Separation and Purification Technology 191 (2018) 392–399

Contents lists available at ScienceDirect

Separation and Purification Technology

journal homepage: www.elsevier.com/locate/seppur

Short Communication

A Maxwell-Stefan-Glueckauf description of transient mixture uptake in microporous adsorbents

Rajamani Krishna

Van 't Hoff Institute for Molecular Sciences, University of Amsterdam, Science Park 904, 1098 XH Amsterdam, The Netherlands

ARTICLE INFO

Keywords:
Transient mixture uptake
Microporous adsorbents
Fick diffusion
Maxwell-Stefan diffusion
Thermodynamic coupling
Linearized driving force

ABSTRACT

Based on the assumptions of uncoupled diffusion fluxes and loading-independent Fick diffusivities, the linear driving force (LDF) model developed by Glueckauf finds widespread usage in the modelling of transient mixture uptake in microporous adsorbents. A number of experimental investigations report overshoots in intra-crystalline loadings of the more mobile species during transient binary mixture uptake in microporous adsorbents; these overshoots are not anticipated in the classic Glueckauf approach. The origins of the overshoots are traceable to strong coupling between species transfers engendered by mixture adsorption equilibrium thermodynamics; such coupling effects are most conveniently described by the Maxwell-Stefan (M-S) diffusion formulation. In this article, an explicit analytic model is developed to calculate transient mixture uptakes by combining the Maxwell-Stefan formulation with the linearization procedure of Glueckauf. The Maxwell-Stefan-Glueckauf model is validated by comparison with six different experimental data sets. In all six cases, the overshoots in the uptake of the more mobile partner species are properly captured; the incorporation of this approach in practical design procedures for adsorbers is expected to result in significant reduction in model complexity and computational times.

1. Introduction

Microporous adsorbents such as zeolites, carbon molecular sieves (CMS), metal-organic frameworks (MOFs), and zeolitic imidazolate framework (ZIFs) have potential applications in a wide variety of separation applications, that are commonly conducted in fixed bed devices. These devices are operated in a cyclical manner, with adsorption and desorption cycles [1–6]. The concentrations of the constituent species in the bulk fluid phase vary with position z along the bed, and time, t; see schematic in Fig. 1. At any position z in the fixed bed, and time t, the molar loadings in the adsorbed phase within the pores, varies along the radius of the particle, r. Most commonly, the separation performance in a fixed-bed adsorber is dictated by mixture adsorption equilibrium. Intra-particle diffusion limitations cause distended breakthrough characteristics and usually lead to diminished separation effectiveness [2,3]. However, there are some instances of diffusion-selective operations in which diffusional effects over-ride the influence of mixture adsorption equilibrium and is the prime driver for separations [1,4,5,7]. Examples of diffusion-selective separations include: (1) selective uptake of N_2 from N_2/CH_4 mixtures using LTA-4A zeolite and Ba-ETS-4 [8–10], and (2) selective uptake of O_2 from O_2/N_2 mixtures using LTA-4A zeolite and CMS [5,11–14]. The development of such diffusion-selective processes requires accurate and robust models to describe transient mixture uptake within the adsorbent particles; the prime focus of this article is the development of such models. To set the scene, and define our objectives, we begin by examining the commonly used modelling approaches.

The spatio-temporal distribution of molar loadings, q_i, within a spherical crystallite particle, of radius r_c, is obtained from a solution of a set of differential equations describing the transient uptake

$$\rho\frac{\partial q_i(r,t)}{\partial t} = -\frac{1}{r^2}\frac{\partial}{\partial r}(r^2 N_i); \quad i = 1,2...n \tag{1}$$

The molar fluxes N_i are commonly related to the gradients in the molar loadings by Fick's law

E-mail address: r.krishna@contact.uva.nl.

http://dx.doi.org/10.1016/j.seppur.2017.09.057
Received 10 July 2017; Received in revised form 5 September 2017; Accepted 26 September 2017
Available online 28 September 2017
1383-5866/

Nomenclature

b_i	Langmuir constant for species i, Pa^{-1}
$[B]$	matrix of inverse M-S coefficients, defined by Eq. (13), m^{-2} s
$Đ_i$	Maxwell-Stefan diffusivity for molecule-wall interaction, m^2 s^{-1}
$Đ_{ij}$	M-S exchange coefficient for n-component mixture, m^2 s^{-1}
$Đ_{12}$	M-S exchange coefficient for binary mixture, m^2 s^{-1}
$[D]$	matrix of Fick diffusivities, m^2 s^{-1}
f_i	partial fugacity of species i, Pa
n	number of species in the mixture, dimensionless
N_i	molar flux of species i with respect to framework, mol m^{-2} s^{-1}
p_i	partial pressure of species i in mixture, Pa
p_t	total system pressure, Pa
q_i	component molar loading of species i, mol kg^{-1}
$q_{i,sat}$	molar loading of species i at saturation, mol kg^{-1}
q_t	total molar loading in mixture, mol kg^{-1}
$\bar{q}_i(t)$	spatial-averaged component uptake of species i, mol kg^{-1}
$[Q]$	matrix defined in Eqs. (17) or (20), dimensionless
r	radial direction coordinate, m
r_c	radius of crystallite, m
R	gas constant, 8.314 J mol^{-1} K^{-1}
t	time, s
T	absolute temperature, K
x_i	mole fraction of species i in adsorbed phase, dimensionless
z	distance coordinate, m

Greek letters

Γ_{ij}	thermodynamic factors, dimensionless
$[\Gamma]$	matrix of thermodynamic factors, dimensionless
θ_i	fractional occupancy of component i, dimensionless
μ_i	molar chemical potential of component i, J mol^{-1}
ρ	framework density, kg m^{-3}

Subscripts

i	referring to component i
t	referring to total mixture
sat	referring to saturation conditions

$$N_i = -\rho D_i \frac{\partial q_i}{\partial r}; \quad i = 1,2...n \tag{2}$$

An analytic solution to Eqs. (1) and (2) can be derived for the special case in which the following three constraints are satisfied: (1) the Fick diffusivity D_i for each of the components can be considered to be independent of the loading, (2) the initial locations at all locations r within the crystal are uniform, i.e. $q_i(r,0) = q_i(r_c,0)$, and (3) for all times $t \geq 0$, the exterior of the crystal is brought into contact with a bulk fluid mixture at partial fugacities $f_i(r_c,t)$ that is maintained constant till the crystal reaches thermodynamic equilibrium with the surrounding fluid mixture. The analytic solution, derived first by Geddes [15] to describe diffusion inside spherical vapor bubbles on distillation trays, is expressed as

$$\frac{(q_i^* - \bar{q}_i(t))}{(q_i^* - q_i(r_c,0))} = \frac{6}{\pi^2} \sum_{m=1}^{\infty} \frac{\exp\left(-m^2\pi^2 \frac{D_i}{r_c^2} t\right)}{m^2} \tag{3}$$

where the spatial-averaged component loading at time t is

$$\bar{q}_i(t) = \frac{3}{r_c^3} \int_0^{r_c} q_i(r,t) r^2 dr \tag{4}$$

and q_i^* is the molar loading that is in equilibrium with the bulk fluid mixture.

In his classic paper, Glueckauf [16] derived the following simplified relation

$$\rho \frac{\partial \bar{q}_i(t)}{\partial t} = -\frac{15 D_i}{r_c^2} (q_i^* - \bar{q}_i(t)); \quad i = 1,2...n \tag{5}$$

that is valid for the condition $\frac{D_i t}{r_c^2} > 0.1$, along with the assumption $\frac{\partial \bar{q}_i(t)}{\partial t} \approx \frac{\partial q_i^*}{\partial t}$. The Glueckauf expression (5) is commonly referred to as the linear driving force (LDF) model. Sircar and Hufton [17,18] provide a fundamental rationalization for its widespread and successful use; they also take the view that the value of the constant need not be restricted to 15, and may be fitted match experiments.

The LDF model predicts that each component will approach equilibrium following

$$\frac{(q_i^* - \bar{q}_i(t))}{(q_i^* - q_i(r_c,0))} = \exp\left(-\frac{15 D_i}{r_c^2} t\right); \quad i = 1,2...n \tag{6}$$

Since the Fick diffusivities are assumed to be loading independent, Eq. (6) also implies that the approach to equilibrium for each species will be monotonous, i.e. without overshoots or undershoots.

Fig. 2 provides a compilation of experimental data on the transient spatially-averaged component loadings during transient uptake in four different host materials. In their experimental investigations using interference microscopy (IFM), Binder et al. [19] and Lauerer et al. [20] have monitored the uptake of CO_2, and C_2H_6 within crystals of DDR zeolite exposed to a bulk gas phase consisting of 1:1, 2:1, and 3:1 CO_2/C_2H_6 mixtures. In the three sets of experiments, overshoots in CO_2 loadings are observed during transient equilibration; see Fig. 2a–c. These experiments suggest the feasibility of devising a diffusion-selective process for selective adsorption of CO_2 from mixtures with ethane; see Fig. S5.

For transient uptake of N_2/CH_4 mixtures, overshoots in the loading of the more mobile N_2 have been reported for LTA-4A zeolite by Habgood [8]; see Fig. 2d. The experimental data of Saint-Remi et al. [21] for transient uptake of ethanol/1-propanol mixtures within SAPO-34, that is the structural analog of CHA zeolite, are shown in Fig. 2e; the more mobile ethanol is found to exhibit a pronounced maximum during the uptake transience. The experimental data of Titze et al. [22] for transient uptake of n-hexane(nC6)/2-methylpentane(2MP) mixtures in MFI zeolite crystal, exposed to an equimolar binary gas mixture at constant total pressure, shows a pronounced overshoot in the uptake of the more mobile linear isomer nC6; see Fig. 2f. In all the foregoing examples, the attainment of supra-equilibrium loadings signals uphill diffusion [23]. For all six data sets, the use of Eq. (6), shown by the dashed lines, fails to capture the overshoots in the uptake of the more mobile partner species.

In a detailed analysis of these experimental data sets, Krishna [24] has demonstrated that the overshoots are caused by coupled species transfers, engendered by mixture adsorption thermodynamics. For quantitative modelling of transient uptakes it is necessary to adopt the

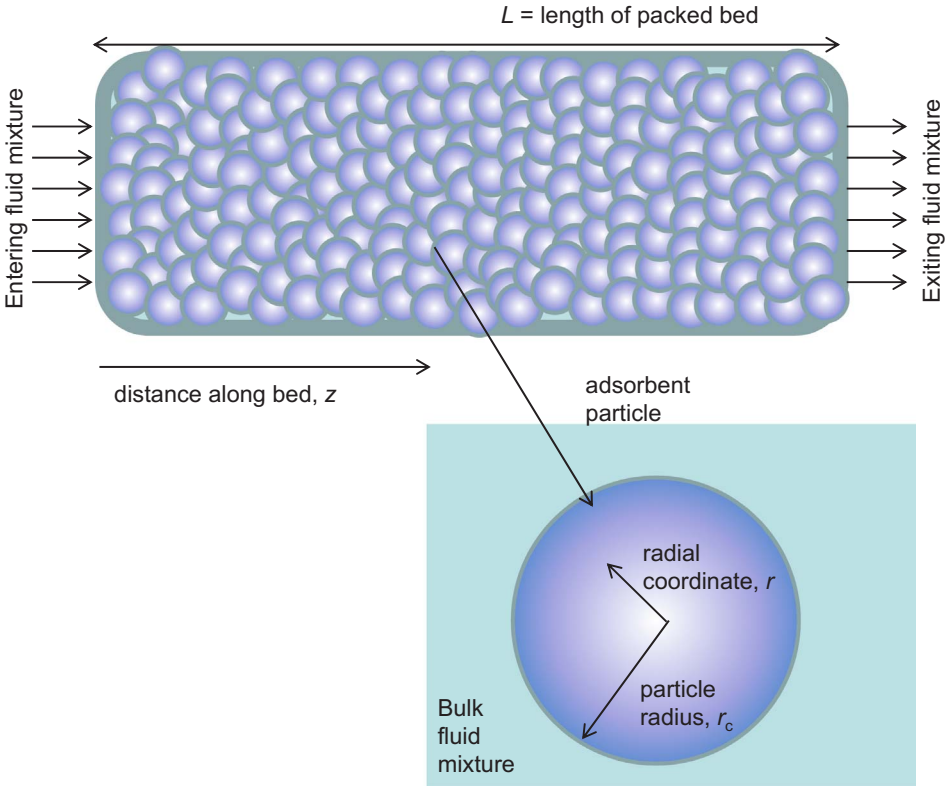

Fig. 1. Schematic of fixed bed adsorber filled with adsorbent particles of radius r_c.

Maxwell-Stefan (M-S) diffusion formulation in which the molar fluxes N_i are related to the gradients of the chemical potential:

$$-\rho\frac{q_i}{RT}\frac{\partial\mu_i}{\partial r} = \sum_{\substack{j=1\\ j\neq i}}^{n}\left(\frac{x_jN_i - x_iN_j}{Đ_{ij}}\right) + \frac{N_i}{Đ_i}; \quad i = 1,2...n \tag{7}$$

The x_i in Eq. (7) represent the component mole fractions in the adsorbed phase within the pores $x_i = q_i/q_t$; $q_t = \sum_{i=1}^{n} q_i$; $i = 1,2,...n$. The $Đ_i$ have the same significance as for unary diffusion; they are inverse drag coefficients between the species i and the pore walls; these diffusivities are determinable from unary uptake experiments.

The Onsager reciprocal relations demand the symmetry constraint

$$Đ_{ij} = Đ_{ji}; \quad i,j = 1,2,...n \tag{8}$$

The $Đ_{ij}$ may be interpreted as the inverse drag coefficient between species i and species j. At the molecular level, the $Đ_{ij}$ reflect how the facility for transport of species i *correlates* with that of species j; they are also termed *exchange coefficients*. The first members on the right hand side of Eq. (7) are required to quantify slowing-down effects that characterize binary mixture diffusion; slowing-down is caused because the jumps of the more mobile species are correlated with the jumps of the tardier partner species [25–27]. The exchange coefficients $Đ_{ij}$ cannot be determined directly from experiments. In some simple cases, use of Molecular Dynamics (MD) simulations [2,25–31] allow some insights to be gained on the characteristics of $Đ_{ij}$.

Generally, the set of Eqs. (1), (4) and (7) need to be solved numerically [24]; these are shown by the dotted lines in Fig. 2. The numerical solution is able to quantitatively capture the transient overshoots in all cases. Since the description of transient uptake within a single particle forms a subset of the overall model for a fixed bed adsorber (see Fig. 1), the implementation of the M-S formulation for intracrystalline diffusion is a challenging task, requiring the use of robust computational routines as detailed in earlier works [2,24]. The primary objective of this communication is to develop an explicit procedure to determine the transient uptake by developing analytic solutions to the M-S equations by a matrix generalization of the Glueckauf LDF approximation. Though the developed matrix relations are formally valid for n-component uptakes, the procedure is illustrated below for binary ($n = 2$) mixtures.

2. The Maxwell-Stefan-Glueckauf model development and results

For binary mixture diffusion, the Maxwell-Stefan Eq. (7) are written as

$$\begin{aligned} -\rho\frac{q_1}{RT}\frac{\partial\mu_1}{\partial r} &= \frac{x_2N_1 - x_1N_2}{Đ_{12}} + \frac{N_1}{Đ_1}\\ -\rho\frac{q_2}{RT}\frac{\partial\mu_2}{\partial r} &= \frac{x_1N_2 - x_2N_1}{Đ_{12}} + \frac{N_2}{Đ_2} \end{aligned} \tag{9}$$

The gradients in the chemical potential can be related to the gradients of the molar loadings by defining thermodynamic correction factors Γ_{ij}

$$\frac{q_i}{RT}\frac{\partial\mu_i}{\partial r} = \sum_{j=1}^{n2}\Gamma_{ij}\frac{\partial q_j}{\partial r}; \qquad \Gamma_{ij} = \frac{q_i}{f_i}\frac{\partial f_i}{\partial q_j}; \qquad i,j = 1,2 \tag{10}$$

where f_i are the partial fugacities in the bulk fluid mixture. The thermodynamic correction factors Γ_{ij} can be calculated by differentiation of the model describing mixture adsorption equilibrium. Generally speaking, the Ideal Adsorbed Solution Theory (IAST) of Myers and Prausnitz [32] is the preferred method for estimation of mixture adsorption equilibrium. In some special cases, the mixed-gas Langmuir model

$$\frac{q_1}{q_{1,sat}} = \theta_1 = \frac{b_1p_1}{1 + b_1p_1 + b_2p_2}; \quad \frac{q_2}{q_{2,sat}} = \theta_2 = \frac{b_2p_2}{1 + b_1p_1 + b_2p_2} \tag{11}$$

may be of adequate accuracy. For CO_2/C_2H_6 mixture adsorption in DDR zeolite, detailed comparison with IAST shows that the mixed-gas Langmuir model has been shown to be of good accuracy [24]. For the mixed-gas Langmuir model, Eq. (11), we can derive simple analytic expressions for the four elements of the matrix of thermodynamic factors [Γ]:

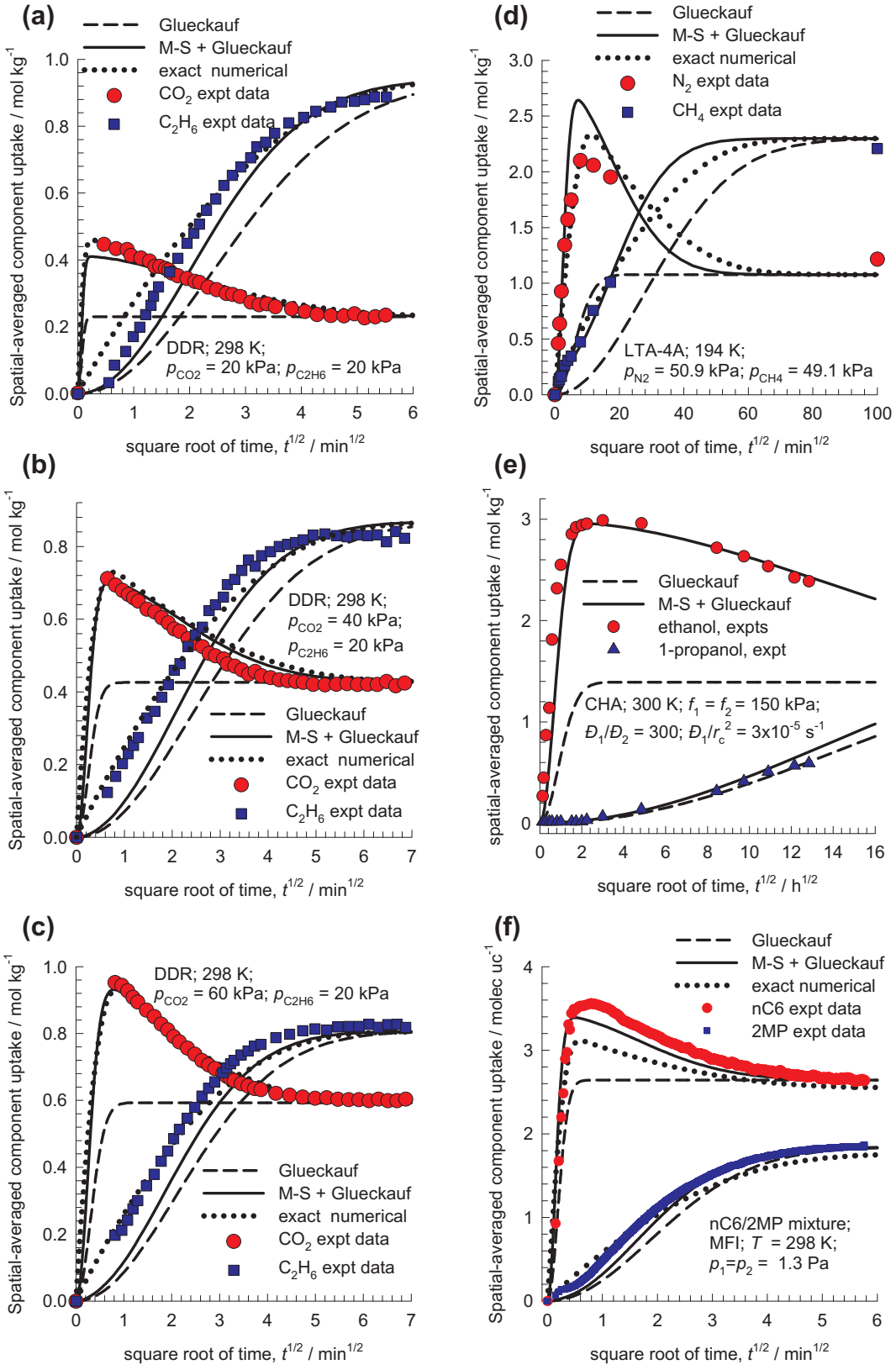

Fig. 2. (a–c) Experimental data of Binder et al. [19] and Lauerer et al. [20] (indicated by symbols) for spatial-averaged transient uptake of (a) 1:1 (b) 2:1, and (c) 3:1 $CO_2(1)/C_2H_6(2)$ gas mixtures within crystals of DDR zeolite at 298 K. (d) Experimental data of Habgood [8] on transient uptake of $N_2(1)/CH_4(2)$ mixture within LTA-4A crystals, exposed to binary gas mixtures at 194 K and partial pressures $p_1 = 50.9$ kPa; $p_2 = 49.1$ kPa. (e) Experimental data of Saint-Remi et al. [21] for transient uptake of ethanol/1-propanol mixtures within SAPO-34, that is the structural analog of CHA zeolite. (f) Experimental data (Run 1) of Titze et al. [22] for transient uptake of 50/50 nC6/2MP mixtures in MFI zeolite at 298 K and total pressure of 2.6 Pa. The dashed lines are the calculations using the classic Glueckauf model. The continuous solid lines are calculations based on the Maxwell-Stefan-Glueckauf model, developed in this work. The dotted lines are the calculations using the exact numerical solutions, as reported in the publication of Krishna [24]. All data inputs on isotherms and diffusivities are provided in the Supplementary material. Video animations 1–6 of the spatio-temporal development of component loadings have been uploaded as Supplementary material.

$$\begin{bmatrix} \Gamma_{11} & \Gamma_{12} \\ \Gamma_{21} & \Gamma_{22} \end{bmatrix} = \frac{1}{1-\theta_1-\theta_2}\begin{bmatrix} 1-\theta_2 & \frac{q_{1,sat}}{q_{2,sat}}\theta_1 \\ \frac{q_{2,sat}}{q_{1,sat}}\theta_2 & 1-\theta_1 \end{bmatrix} \tag{12}$$

where the fractional occupancies, θ_i, are defined by Eq. (11). The elements of the matrix of thermodynamic factors Γ_{ij} can be calculated explicitly from information on the component loadings q_i in the adsorbed phase; this is the persuasive advantage of the use of the mixed-gas Langmuir model. By contrast, the IAST does not allow the calculation of Γ_{ij} explicitly from knowledge on the component loadings q_i in the adsorbed phase; an implicit solution procedure is required. Even if the IAST is used to calculate the mixture adsorption equilibrium, the use of Eq. (12) to calculate the elements of the matrix of thermodynamic factors is a good approximation; evidence of this is provided by Krishna [24], for CO_2/C_2H_6 mixture adsorption in DDR zeolite.

For analysis of the systems in which the saturation capacities are different, the IAST has been consistently used in this work for calculation of mixture adsorption equilibrium for mixtures.

We define the square matrix $[B]$ as

$$[B] = \begin{bmatrix} \frac{1}{Đ_1} + \frac{x_2}{Đ_{12}} & -\frac{x_1}{Đ_{12}} \\ -\frac{x_2}{Đ_{12}} & \frac{1}{Đ_2} + \frac{x_1}{Đ_{12}} \end{bmatrix} \tag{13}$$

A 2 × 2 dimensional Fick diffusivity matrix $[D]$ is defined as the product of $[B]^{-1}$ and the matrix of thermodynamic correction factors $[\Gamma]$:

$$[D] = [B]^{-1}[\Gamma] = \frac{1}{1+\frac{x_1Đ_2}{Đ_{12}}+\frac{x_2Đ_1}{Đ_{12}}}\begin{bmatrix} Đ_1\left(1+\frac{x_1Đ_2}{Đ_{12}}\right) & \frac{x_1Đ_1Đ_2}{Đ_{12}} \\ \frac{x_2Đ_1Đ_2}{Đ_{12}} & Đ_2\left(1+\frac{x_2Đ_1}{Đ_{12}}\right) \end{bmatrix}\begin{bmatrix} \Gamma_{11} & \Gamma_{12} \\ \Gamma_{21} & \Gamma_{22} \end{bmatrix} \tag{14}$$

For unary diffusion, Eq. (14) degenerates to the familiar scalar equation $D = Đ\Gamma$. Correlation effects are of negligible importance for mixture diffusion in cage-type hosts such as LTA, DDR, CHA, ERI, and ZIF-8 that consist of cages separated by narrow windows in the 3.3–4.4 Å size range; the molecules hop one-at-a-time between cages [25–27,33]. In this scenario, $Đ_1 \ll Đ_{12}$; $Đ_2 \ll Đ_{12}$, and Eq. (14) simplifies to yield

$$[D] = \begin{bmatrix} Đ_1 & 0 \\ 0 & Đ_2 \end{bmatrix}\begin{bmatrix} \Gamma_{11} & \Gamma_{12} \\ \Gamma_{21} & \Gamma_{22} \end{bmatrix} \tag{15}$$

Combining Eqs. (9), (10), (13) and (14), we obtain the following explicit expression for the fluxes, expressed in 2-dimensional matrix notation as

$$(N) = -\rho[D]\frac{\partial(q)}{\partial r} \tag{16}$$

For the uptake of CO_2/C_2H_6 mixtures in DDR, N_2/CH_4 mixtures in LTA-4A, ethanol/1-propanol uptake in SAPO-34, Eq. (15) is the appropriate expression for the Fick diffusivity matrix $[D]$. By detailed consideration of correlation effects for nC6/2MP uptake in MFI zeolite, Titze et al. [22] have established the validity of Eq. (15) to model intra-crystalline fluxes. Since the matrix $[\Gamma]$ is determined from mixture adsorption equilibrium, the modelling of all six data sets in Fig. 2 requires input data on just two parameters: $Đ_1/r_c^2$, and $Đ_2/r_c^2$; these input data are provided in the Supplementary Material.

The Fick diffusivity matrix $[D]$ is a function of component loadings, and in the development of the linearized model, we determine the value of the $[D]$ at the component loadings in equilibrium with the bulk fluid mixture, q_i^*; this diffusivity matrix is taken to be constant for the duration of the equilibration process. The matrix generalization of the Geddes Eq. (3) for constant $[D]$ is discussed in detail in Chapter 9 of Taylor and Krishna [34]; the result is

$$(q^* - \bar{q}(t)) = [Q](q^* - q_0); \quad [Q] \equiv \frac{6}{\pi^2}\sum_{m=1}^{\infty}\frac{1}{m^2}\exp\left[-m^2\pi^2\frac{[D]t}{r_c^2}\right] \tag{17}$$

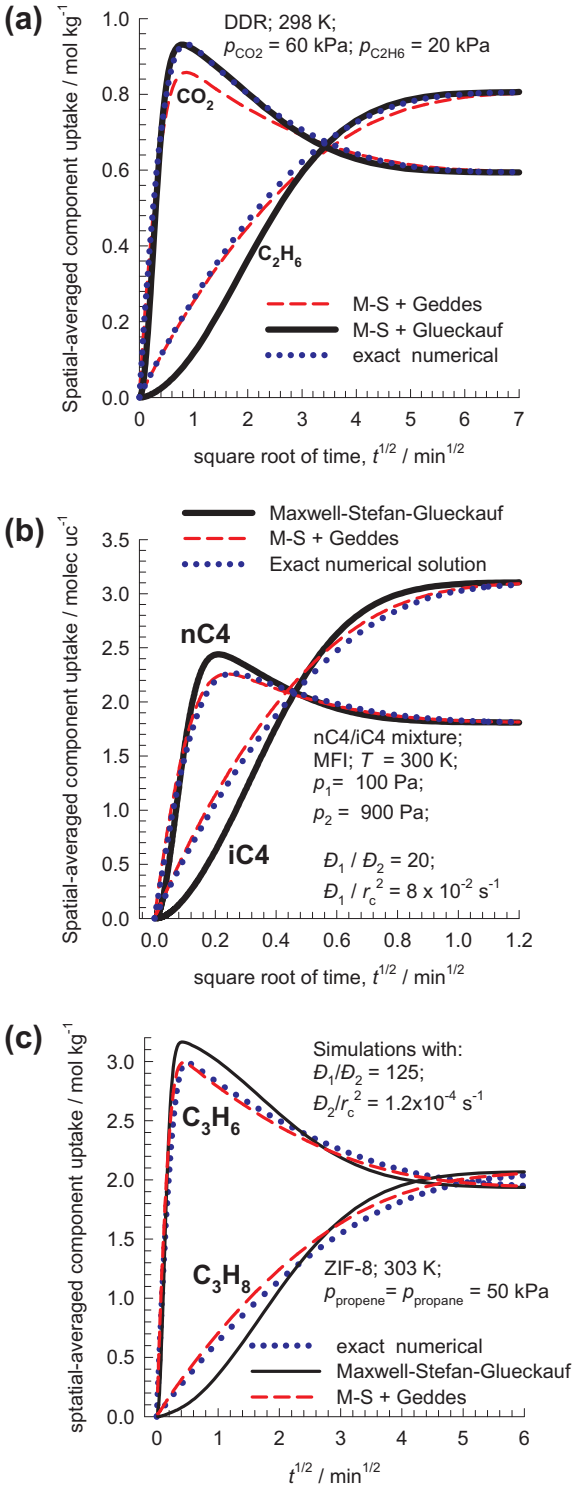

Fig. 3. Comparison of three different models for calculations of transient uptake of (a) 3:1 $CO_2(1)/C_2H_6(2)$ gas mixtures within crystals of DDR zeolite at 298 K, and (b) 1:9 n-butane(nC4)/i-butane(iC4) mixtures in MFI zeolite at 300 K, and (c) 1:1 C_3H_6/C_3H_8 mixtures in ZIF-8 at 303 K. The dashed lines are the calculations using the Maxwell-Stefan-Geddes model. The continuous solid lines are calculations based on the Maxwell-Stefan-Glueckauf model, developed in this work. The dotted lines are the calculations using the exact numerical solutions, as reported in the publication of Krishna [24].

In Eq. (17), (q_0), (q^*), $(\bar{q}(t))$ represent, respectively, the 2-dimensional column matrices of component loadings corresponding to: initial conditions (zero for all the experiments shown in Fig. 2), at final equilibrium, and spatially-averaged values at time t. The Sylvester theorem,

detailed in Appendix A of Taylor and Krishna [34], is required for explicit calculation of the 2 × 2 dimensional matrix [Q]. For the case of distinct eigenvalues, λ_1 and λ_2 of the Fick diffusivity matrix [D], the Sylvester theorem yields

$$[Q] = \frac{f(\lambda_1)[[D]-\lambda_2[I]]}{(\lambda_1-\lambda_2)} + \frac{f(\lambda_2)[[D]-\lambda_1[I]]}{(\lambda_2-\lambda_1)} \quad (18)$$

in which $f(\lambda_i) = \frac{6}{\pi^2}\sum_{m=1}^{\infty}\frac{1}{m^2}\exp\left[-m^2\pi^2\frac{\lambda_i t}{r_c^2}\right]; \quad i = 1,2.$

If both the eigenvalues satisfy the condition $\frac{\lambda_i t}{r_c^2} > 0.1$, the matrix generalization of the Glueckauf expressions (5) and (6) are, respectively,

$$\rho\frac{\partial(\overline{q}(t))}{\partial t} = -\frac{15[D]}{r_c^2}(q^*-\overline{q}(t)) \quad (19)$$

and

$$(q^*-\overline{q}(t)) = [Q](q^*-q_0); \quad [Q] \equiv \exp\left[-\frac{15[D]t}{r_c^2}\right] \quad (20)$$

For evaluation of [Q] in Eq. (20), we apply Eq. (18), taking $f(\lambda_i) = \exp\left[-\frac{15\lambda_i t}{r_c^2}\right]; \quad i = 1,2.$

As illustration, Fig. 3a presents a comparison of three different models for calculations of transient uptake of 3:1 $CO_2(1)/C_2H_6(2)$ gas mixtures within crystals of DDR zeolite at 298 K. The dotted lines are the calculations using the exact numerical solutions, as reported in the publication of Krishna [24]. The dashed lines are the calculations using the Geddes model, Eq. (17). We note that the analytic Geddes model is in reasonably good agreement with the exact numerical solution; this validates the matrix generalization procedure used to derive Eq. (17). The continuous solid lines are calculations based on Eq. (20), dubbed the Maxwell-Stefan-Glueckauf model; the obtained results for C_2H_6 loading is slightly less accurate than the exact numerical solution. Similar good agreement between the Maxwell-Stefan-Glueckauf model and exact numerical solutions is obtained for uptake of n-butane(nC4)/i-butane(iC4) in MFI zeolite (see Fig. 3b), C_3H_6/C_3H_8 in ZIF-8 (see Fig. 3c), O_2/N_2 in LTA-4A (see Fig. S12), and Kr/Xe uptake in SAPO-34 (see Fig. S16).

In Fig. 2, the continuous solid lines represent the calculations of the transient uptake using Eq. (20). In all six cases, the transient overshoots of the more mobile partner species are adequately captured, especially for the more mobile partner; the predictions for the tardier component is somewhat poorer because of slower equilibration. In comparison with the exact numerical solutions, presented in our earlier work [24], the agreement of the Maxwell-Stefan-Glueckauf model with experimental data is somewhat inferior. The linearization approximation used in deriving Eq. (20) may be of acceptable accuracy for implementation in process design of fixed bed adsorption devices.

3. Conclusions

The linear driving force (LDF) approximation developed by Glueckauf has been extended to include coupled diffusion effects by using the Maxwell-Stefan diffusion formulation. The key results of this work are Eqs. (19) and (20) that represent formal matrix generalizations of the commonly used Glueckauf formulations based on Fick's law. The implementation of the Maxwell-Stefan-Glueckauf model is straightforward, and involves only explicit numerical calculations requiring the use of Sylvester's formula (18). For the variety of cases examined, there is only a small sacrifice of computational accuracy in simulations of transient uptakes.

Another important message that emerges from this communication, is the necessity of including thermodynamic coupling effects, quantified by the matrix [Γ], in the calculation of the intra-crystalline transfer fluxes. The classic Glueckauf model essentially asserts that [Γ] equals the identity matrix; with this assumption, the transient overshoots of the more mobile species disappear. Interestingly, for the investigated guest/host combinations, transient permeation across membranes results in flux overshoots of the more mobile partners; see Figs. S4, S15, and S17.

Transient breakthrough simulations in fixed bed adsorbers carrying out diffusion-selective separations of CO_2/C_2H_6 mixtures with DDR zeolite (see Fig. S5), and N_2/CH_4 mixtures using LTA-4A zeolite (see Fig. S7) demonstrate that ignoring the influence of [Γ] leads to reduced productivities and separation capability.

Appendix A. Supplementary material

Supplementary data associated with this article can be found, in the online version, at http://dx.doi.org/10.1016/j.seppur.2017.09.057.

References

[1] D.M. Ruthven, S. Farooq, K.S. Knaebel, Pressure Swing Adsorption, VCH Publishers, New York, 1994.
[2] R. Krishna, The Maxwell-Stefan description of mixture diffusion in nanoporous crystalline materials, Microporous Mesoporous Mater. 185 (2014) 30–50.
[3] R. Krishna, Methodologies for evaluation of metal-organic frameworks in separation applications, RSC Adv. 5 (2015) 52269–52295.
[4] R.T. Yang, Gas Separation by Adsorption Processes, Butterworth, Boston, 1987.
[5] R.T. Yang, Adsorbents: Fundamentals and Applications, John Wiley & Sons Inc, Hoboken, New Jersey, 2003.
[6] R. Krishna, Screening metal-organic frameworks for mixture separations in fixed-bed adsorbers using a combined selectivity/capacity metric, RSC Adv. 7 (2017) 35724–35737.
[7] J. Kärger, D.M. Ruthven, D.N. Theodorou, Diffusion in Nanoporous Materials, Wiley-VCH, Weinheim, 2012.
[8] H.W. Habgood, The Kinetics of molecular sieve action. Sorption of nitrogen-methane mixtures by Linde molecular sieve 4A, Canad. J. Chem. 36 (1958) 1384–1397.
[9] S.J. Bhadra, S. Farooq, Separation of methane nitrogen mixture by pressure swing adsorption for natural gas upgrading, Ind. Eng. Chem. Res. 50 (2011) 14030–14045.
[10] B. Majumdar, S.J. Bhadra, R.P. Marathe, S. Farooq, Adsorption and diffusion of methane and nitrogen in barium exchanged ETS-4, Ind. Eng. Chem. Res. 50 (2011) 3021–3034.
[11] S. Farooq, M.N. Rathor, K. Hidajat, A predictive model for a kinetically controlled pressure swing adsorption separation process, Chem. Eng. Sci. 48 (1993) 4129–4141.
[12] S. Farooq, Sorption and diffusion of oxygen and nitrogen in molecular sieve RS-10, Gas Sep. Purif. 9 (1995) 205–212.
[13] Y.D. Chen, R.T. Yang, P. Uawithya, Diffusion of oxygen, nitrogen and their mixtures in carbon molecular-sieve, AIChE J. 40 (1994) 577–585.
[14] S. Sircar, A.L. Myers, Gas Separation by Zeolites, in: M. Auerbach, K.A. Carrado, P.K. Dutta (Eds.), Handbook of Zeolite Science and Technology, Marcel Dekker, New York, 2003, pp. 1063–1104 (Chapter 22).
[15] R.L. Geddes, Local efficiencies of bubble-plate fractionators, Trans. Am. Inst. Chem. Engrs. 42 (1946) 79–105.
[16] E. Glueckauf, Theory of chromatography. Part 10 – Formulae for diffusion into spheres and their application to chromatography, Trans. Faraday Soc. 51 (1955) 1540–1551.
[17] S. Sircar, J.R. Hufton, Why does the Linear Driving Force model for adsorption kinetics work ? Adsorption 6 (2000) 137–147.
[18] S. Sircar, J.R. Hufton, Intraparticle adsorbate concentration profile for linear driving force model, AIChE J. 46 (2000) 659–660.
[19] T. Binder, A. Lauerer, C. Chmelik, J. Haase, J. Kärger, D.M. Ruthven, Micro-imaging of transient intracrystalline concentration profiles during two-component uptake of light hydrocarbon - carbon dioxide mixtures by DDR-type zeolites, Ind. Eng. Chem. Res. 54 (2015) 8997–9004.
[20] A. Lauerer, T. Binder, C. Chmelik, E. Miersemann, J. Haase, D.M. Ruthven, J. Kärger, Uphill diffusion and overshooting in the adsorption of binary mixtures in nanoporous solids, Nat. Commun. 6 (2015) 7697, http://dx.doi.org/10.1038/ncomms8697.
[21] J.C. Saint-Remi, G.V. Baron, J.F.M. Denayer, Non-uniform chain length dependent diffusion of short 1-alcohols in SAPO-34 in liquid phase, J. Phys. Chem. C 117 (2013) 9758–9765.
[22] T. Titze, C. Chmelik, J. Kärger, J.M. van Baten, R. Krishna, Uncommon synergy between adsorption and diffusion of hexane isomer mixtures in MFI zeolite induced by configurational entropy effects, J. Phys. Chem. C 118 (2014) 2660–2665.
[23] R. Krishna, Uphill Diffusion in multicomponent mixtures, Chem. Soc. Rev. 44 (2015) 2812–2836.
[24] R. Krishna, Tracing the origins of transient overshoots for binary mixture diffusion in microporous crystalline materials, Phys. Chem. Chem. Phys. 18 (2016) 15482–15495.
[25] R. Krishna, Describing the diffusion of guest molecules inside porous structures, J.

Phys. Chem. C 113 (2009) 19756–19781.
[26] R. Krishna, Diffusion in porous crystalline materials, Chem. Soc. Rev. 41 (2012) 3099–3118.
[27] R. Krishna, J.M. van Baten, Investigating the influence of diffusional coupling on mixture permeation across porous membranes, J. Membr. Sci. 430 (2013) 113–128.
[28] R. Krishna, J.M. van Baten, Investigating the relative influences of molecular dimensions and binding energies on diffusivities of guest species inside nanoporous crystalline materials, J. Phys. Chem. C 116 (2012) 23556–23568.
[29] R. Krishna, J.M. van Baten, Influence of adsorption thermodynamics on guest diffusivities in nanoporous crystalline materials, Phys. Chem. Chem. Phys. 15 (2013) 7994–8016.
[30] R. Krishna, J.M. van Baten, Insights into diffusion of gases in zeolites gained from molecular dynamics simulations, Microporous Mesoporous Mater. 109 (2008) 91–108.
[31] R. Krishna, J.M. van Baten, Diffusion of alkane mixtures in MFI zeolite, Microporous Mesoporous Mater. 107 (2008) 296–298.
[32] A.L. Myers, J.M. Prausnitz, Thermodynamics of mixed gas adsorption, AIChE J. 11 (1965) 121–130.
[33] R. Krishna, J.M. van Baten, A molecular dynamics investigation of the diffusion characteristics of cavity-type zeolites with 8-ring windows, Microporous Mesoporous Mater. 137 (2011) 83–91.
[34] R. Taylor, R. Krishna, Multicomponent Mass Transfer, John Wiley, New York, 1993.

Supplementary Material to accompany:

A Maxwell-Stefan-Glueckauf Description of Transient Mixture Uptake in Microporous Adsorbents

Rajamani Krishna

Van 't Hoff Institute for Molecular Sciences, University of Amsterdam, Science Park 904,

1098 XH Amsterdam, The Netherlands

Email: r.krishna@contact.uva.nl

Table of Contents

1. Preamble

This Supplementary Material (SM) accompanying the article *A Maxwell-Stefan-Glueckauf Description of Transient Mixture Uptake in Microporous Adsorbents* provides (a) detailed derivation of the Maxwell-Stefan equations, (b) details of methodology adopted for numerical solutions to transient uptake within single crystalline particle, (c) details of methodology used for transient breakthroughs in fixed bed adsorbers, and (d) input data on pure component isotherms, and Maxwell-Stefan diffusivities for simulations of the experimental data sets.

Video animations

The following set of six video animations have also been uploaded as Supplementary material (e-components).

(1) Transient development of loadings of 3:1 CO_2/C_2H_6 in DDR crystal at 298 K. CO_2 exhibits spatio-temporal overshoots.

(2) Transient development of loadings of N_2/CH_4 uptake in LTA-4A at 194 K: simulation of Habgood experiment. N_2 exhibits spatio-temporal overshoots.

(3) Transient development of loadings of nC6/2MP in MFI at 298 K, simulation of Run 1 of Titze. nC6 exhibits spatio-temporal overshoots.

(4) Transient development of ethanol/1-propanol loadings in CHA zeolite. Ethanol exhibits spatio-temporal overshoots.

(5) Transient development of C_3H_6/C_3H_8 loadings in ZIF-8. C_3H_6 exhibits spatio-temporal overshoots.

(6) Transient development of Kr/Xe uptake in SAPO-34. Kr exhibits spatio-temporal overshoots.

2. The Maxwell-Stefan relations for *n*-component diffusion in micropores

The force acting per mole of adsorbate species *i* is balanced by (1) friction between *i* and the pore walls (this is the same term as for unary transport), and (2) friction between species *i* and species *j*. We may write

$$-\frac{1}{RT}\frac{\partial \mu_i}{\partial r} = \sum_{\substack{j=1 \\ j\neq i}}^{n} \frac{x_j}{Đ_{ij}}\left(u_i - u_j\right) + \frac{1}{Đ_i}\left(u_i\right); \quad i = 1,2..n \tag{1}$$

The x_i in equations (1) represent the component mole fractions in the adsorbed phase within the pores

$$x_i = q_i / q_t; \quad q_t = \sum_{i=1}^{n} q_i; \quad i = 1,2,..n \tag{2}$$

The $Đ_i$ have the same significance as for unary diffusion; they are inverse drag coefficients between the species *i* and the material surface. Indeed, an important persuasive advantage of the M-S equations is that the $Đ_i$ for mixture diffusion often retains the same magnitude and loading dependence as for unary diffusion.[1-3]

The $Đ_{ij}$ may be interpreted as the inverse drag coefficient between species *i* and species *j*. At the molecular level, the $Đ_{ij}$ reflect how the facility for transport of species *i correlates* with that of species *j*; they are also termed *exchange coefficients*. The multiplication factor x_j has been introduced in the numerator of the first right member of equation (1) because the friction experience by species *i* with the each of the other species in the adsorbed phase (*j* = 2, 3, ..*n*) should be proportional to the relative amounts of species *j* (= 2, 3, ..*n*) in the adsorbed phase. Expressing the velocities u_j in terms of the intra-crystalline diffusion fluxes $u_i = N_i / \rho q_i$

$$-\frac{\rho}{RT}\frac{\partial \mu_i}{\partial r} = \sum_{\substack{j=1 \\ j\neq i}}^{n} \frac{x_j}{Đ_{ij}}\left(\frac{N_i}{q_i} - \frac{N_j}{q_j}\right) + \frac{1}{Đ_i}\left(\frac{N_i}{q_i}\right); \quad i = 1,2...n \tag{3}$$

Multiplying both sides of equation (3) by x_i we get

$$-\rho\frac{x_i}{RT}\frac{\partial\mu_i}{\partial r}=\sum_{\substack{j=1\\ j\neq i}}^{n}\frac{x_i x_j}{Đ_{ij}}\left(\frac{N_i}{q_i}-\frac{N_j}{q_j}\right)+\frac{1}{Đ_i}\left(\frac{x_i N_i}{q_i}\right);\quad i=1,2...n \tag{4}$$

In view of the equation (2), we may simplify equation (4) to write

$$-\rho\frac{q_i}{RT}\frac{\partial\mu_i}{\partial r}=\sum_{\substack{j=1\\ j\neq i}}^{n}\left(\frac{x_j N_i-x_i N_j}{Đ_{ij}}\right)+\frac{N_i}{Đ_i};\quad i=1,2...n \tag{5}$$

The Onsager reciprocal relations demand the symmetry constraint

$$Đ_{ij}=Đ_{ji};\quad i,j=1,2,...n \tag{6}$$

3. The Maxwell-Stefan relations for binary mixture diffusion in micropores

For binary mixture diffusion inside porous crystalline materials the Maxwell-Stefan equations (5) are written as

$$\begin{aligned}-\rho\frac{q_1}{RT}\frac{\partial\mu_1}{\partial r}&=\frac{x_2N_1-x_1N_2}{Đ_{12}}+\frac{N_1}{Đ_1}\\ -\rho\frac{q_2}{RT}\frac{\partial\mu_2}{\partial r}&=\frac{x_1N_2-x_2N_1}{Đ_{12}}+\frac{N_2}{Đ_2}\end{aligned} \tag{7}$$

The first members on the right hand side of Equation (7) are required to quantify slowing-down effects that characterize binary mixture diffusion.[1, 2, 4] There is no experimental technique for direct determination of the exchange coefficients $Đ_{12}$, that quantify molecule-molecule interactions.

For purposes of calculations of the uptake within crystals, we need to calculate the chemical potential gradients, $\frac{\partial\mu_i}{\partial r}$, where r is the radius of a spherical crystal. For an ideal gas mixture, the chemical potential gradients can be related to the partial pressure gradients in the bulk gas phase mixture

$$\frac{\partial\mu_i}{\partial r}=RT\frac{\partial\ln p_i}{\partial r}=RT\frac{1}{p_i}\frac{\partial p_i}{\partial r} \tag{8}$$

The gradients in the chemical potential can be related to the gradients of the molar loadings by defining thermodynamic correction factors Γ_{ij}

$$\frac{q_i}{RT}\frac{\partial \mu_i}{\partial r} = \sum_{j=1}^{2} \Gamma_{ij} \frac{\partial q_j}{\partial r}; \quad \Gamma_{ij} = \frac{q_i}{p_i}\frac{\partial p_i}{\partial q_j}; \quad i, j = 1,2 \tag{9}$$

In 2-dimensional matrix notation, equation (9) takes the form

$$-\begin{pmatrix} \frac{q_1}{RT}\frac{\partial \mu_1}{\partial r} \\ \frac{q_2}{RT}\frac{\partial \mu_2}{\partial r} \end{pmatrix} = [\Gamma] \begin{pmatrix} \frac{\partial q_1}{\partial r} \\ \frac{\partial q_2}{\partial r} \end{pmatrix} \tag{10}$$

The thermodynamic correction factors Γ_{ij} can be calculated by differentiation of the model describing mixture adsorption equilibrium. Generally speaking, the Ideal Adsorbed Solution Theory (IAST) of Myers and Prausnitz[5] is the preferred method for estimation of mixture adsorption equilibrium. In some special case, the mixed-gas Langmuir model

$$\frac{q_1}{q_{1,sat}} = \theta_1 = \frac{b_1 p_1}{1 + b_1 p_1 + b_2 p_2}; \quad \frac{q_2}{q_{2,sat}} = \theta_2 = \frac{b_2 p_2}{1 + b_1 p_1 + b_2 p_2} \tag{11}$$

may be of adequate accuracy.

For the mixed-gas Langmuir model, equation (11), we can derive simple analytic expressions for the four elements of the matrix of thermodynamic factors:[6]

$$\begin{bmatrix} \Gamma_{11} & \Gamma_{12} \\ \Gamma_{21} & \Gamma_{22} \end{bmatrix} = \frac{1}{1 - \theta_1 - \theta_2} \begin{bmatrix} 1 - \theta_2 & \frac{q_{1,sat}}{q_{2,sat}}\theta_1 \\ \frac{q_{2,sat}}{q_{1,sat}}\theta_2 & 1 - \theta_1 \end{bmatrix} \tag{12}$$

where the fractional occupancies, θ_i, are defined by equation (11).

The elements of the matrix of thermodynamic factors Γ_{ij} can be calculated explicitly from information on the component loadings q_i in the adsorbed phase; this is the persuasive advantage of the use of the mixed-gas Langmuir model. By contrast, the IAST does not allow the calculation of Γ_{ij} explicitly from

knowledge on the component loadings q_i in the adsorbed phase; an implicit solution procedure is required. Even if the IAST is used to calculate the mixture adsorption equilibrium, the use of equation (12) to calculate the elements of the matrix of thermodynamic factors is a good approximation. Evidence of this is provided by Krishna[7], for CO_2/C_2H_6 mixture adsorption in DDR zeolite.

Let us define the square matrix [B]

$$[B]=\begin{bmatrix} \frac{1}{Đ_1}+\frac{x_2}{Đ_{12}} & -\frac{x_1}{Đ_{12}} \\ -\frac{x_2}{Đ_{12}} & \frac{1}{Đ_2}+\frac{x_1}{Đ_{12}} \end{bmatrix} \tag{13}$$

Equation (7) can be re-cast into 2-dimensional matrix notation

$$-\rho\begin{pmatrix} \frac{q_1}{RT}\frac{\partial\mu_1}{\partial r} \\ \frac{q_2}{RT}\frac{\partial\mu_2}{\partial r} \end{pmatrix}=[B]\begin{pmatrix} N_1 \\ N_2 \end{pmatrix};\quad \begin{pmatrix} N_1 \\ N_2 \end{pmatrix}=-\rho[B]^{-1}\begin{pmatrix} \frac{q_1}{RT}\frac{\partial\mu_1}{\partial r} \\ \frac{q_2}{RT}\frac{\partial\mu_2}{\partial r} \end{pmatrix} \tag{14}$$

The inverse of the square matrix [B] can be obtained explicitly

$$[B]^{-1}=\frac{1}{1+\frac{x_1Đ_2}{Đ_{12}}+\frac{x_2Đ_1}{Đ_{12}}}\begin{bmatrix} Đ_1\left(1+\frac{x_1Đ_2}{Đ_{12}}\right) & \frac{x_1Đ_1Đ_2}{Đ_{12}} \\ \frac{x_2Đ_1Đ_2}{Đ_{12}} & Đ_2\left(1+\frac{x_2Đ_1}{Đ_{12}}\right) \end{bmatrix} \tag{15}$$

Combining equations (10), (14), and (15) we obtain

$$\begin{pmatrix} N_1 \\ N_2 \end{pmatrix}=-\frac{\rho}{1+\frac{x_1Đ_2}{Đ_{12}}+\frac{x_2Đ_1}{Đ_{12}}}\begin{bmatrix} Đ_1\left(1+\frac{x_1Đ_2}{Đ_{12}}\right) & \frac{x_1Đ_1Đ_2}{Đ_{12}} \\ \frac{x_2Đ_1Đ_2}{Đ_{12}} & Đ_2\left(1+\frac{x_2Đ_1}{Đ_{12}}\right) \end{bmatrix}\begin{bmatrix} \Gamma_{11} & \Gamma_{12} \\ \Gamma_{21} & \Gamma_{22} \end{bmatrix}\begin{pmatrix} \frac{\partial q_1}{\partial r} \\ \frac{\partial q_2}{\partial r} \end{pmatrix} \tag{16}$$

The ratio ($Đ_1/Đ_{12}$) is a reflection of the *degree of correlations*. Extensive Molecular Dynamics (MD) simulations have shown that correlation effects are of negligible importance for mixture diffusion across materials such as LTA, ZIF-8, CHA, DDR, ERI that consist of cages separated by windows in the 3.4 Å

– 4.2 Å size range.[1, 2, 4, 8] Molecules jump one-at-a-time across the narrow windows, and the assumption of negligible correlations is justified.

In cases in which correlations are negligible, Equation (16) simplifies to yield

$$\begin{pmatrix} N_1 \\ N_2 \end{pmatrix} = -\rho \begin{bmatrix} Đ_1 & 0 \\ 0 & Đ_2 \end{bmatrix} \begin{bmatrix} \Gamma_{11} & \Gamma_{12} \\ \Gamma_{21} & \Gamma_{22} \end{bmatrix} \begin{pmatrix} \frac{\partial q_1}{\partial r} \\ \frac{\partial q_2}{\partial r} \end{pmatrix} \tag{17}$$

In the Henry regime of adsorption, when the fractional occupancies are vanishingly small, we have the special case that the matrix of thermodynamic factors reduces to the identity matrix

$$\begin{bmatrix} \Gamma_{11} & \Gamma_{12} \\ \Gamma_{21} & \Gamma_{22} \end{bmatrix} \to \begin{bmatrix} 1 & 0 \\ 0 & 1 \end{bmatrix}; \quad \theta_1, \theta_2 \to 0 \tag{18}$$

If the thermodynamic coupling effects are neglected, and the elements of the matrix of thermodynamic factors Γ_{ij} equals Kronecker delta, $\Gamma_{ij} = \delta_{ij}$ and we obtain the uncoupled form of the flux equations

$$\begin{pmatrix} N_1 \\ N_2 \end{pmatrix} = -\rho \begin{bmatrix} Đ_1 & 0 \\ 0 & Đ_2 \end{bmatrix} \begin{pmatrix} \frac{\partial q_1}{\partial r} \\ \frac{\partial q_2}{\partial r} \end{pmatrix}; \quad \text{neglecting thermodynamic coupling} \tag{19}$$

4. Numerical solutions for transient uptake in microporous particle

For establishing the accuracy of the Maxwell-Stefan-Glueckauf model, comparisons are made with the exact numerical solutions for transient uptake as described in earlier works;[6, 9-11] a brief summary of the methodology is presented hereunder.

The radial distribution of molar loadings, q_i, within a spherical crystallite, of radius r_c, is obtained from a solution of a set of differential equations describing the uptake

$$\rho \frac{\partial q_i(r,t)}{\partial t} = -\frac{1}{r^2} \frac{\partial}{\partial r} \left(r^2 N_i \right) \tag{20}$$

The fluxes N_i, in turn, are related to the radial gradients in the molar loadings by Equation (16), or the simplified Equation (17). At time t = 0, i.e. the initial conditions, the molar loadings $q_i(r,0)$ at all locations r within the crystal are uniform (zero loadings). For all times $t \geq 0$, the exterior of the crystal is brought into contact with a bulk gas mixture at partial pressures $p_i(r_c,t)$ that is maintained constant till the crystal reaches thermodynamic equilibrium with the surrounding gas mixture.

$$t \geq 0; \quad q_i(r_c,t) \text{ in equilibrium with the initial values } p_i(r_c,t) \tag{21}$$

At any time t, during the transient approach to thermodynamic equilibrium, the spatial-averaged component loading within the crystallites of radius r_c is calculated using

$$\bar{q}_i(t) = \frac{3}{r_c^3}\int_0^{r_c} q_i(r,t) r^2 dr \tag{22}$$

The spatial-averaged $\bar{q}_i(t)$ can be compared directly with experimental transient uptake data.

There is no generally applicable analytical solution to describe transient diffusion of binary mixtures and the set of Equations (16), (20), (21), and (22) need to be solved numerically using robust computational techniques. Equations (20) are first subjected to finite volume discretization. One of two strategies can be adopted: (a) equi-volume discretization, or (b) equi-distant discretization; see Figure 1. The choice of the discretization scheme used is crucially important in obtaining accurate, converged results. The choice of equi-volume slices is needed when the gradients of the loadings are particularly steep nearer to $r = r_c$. For either strategy, about 100 – 200 slices were employed in the simulations presented in this work, depending on the guest/host combination. Combination of the discretized partial differential equations (20) along with algebraic equations describing mixture adsorption equilibrium, results in a set of differential-algebraic equations (DAEs), which are solved using BESIRK.[12] BESIRK is a sparse matrix solver, based on the semi-implicit Runge-Kutta method originally developed by Michelsen,[13] and extended with the Bulirsch-Stoer extrapolation method.[14] Use of BESIRK improves the numerical solution efficiency in solving the set of DAEs. The evaluation of the sparse Jacobian

required in the numerical algorithm is largely based on analytic expressions.[6] Further details of the numerical procedures used in this work, are provided by Krishna and co-workers;[6, 9-11] interested readers are referred to our website that contains the numerical details.[9]

5. Simulation methodology for transient breakthrough in fixed bed adsorbers

We describe below the simulation methodology used to perform transient breakthrough calculations for fixed bed adsrobers (see schematic in Figure 1) that are presented in this work. The simulation methodology is the same as used in our earlier publications.[7, 15-17] Assuming plug flow of an *n*-component gas mixture through a fixed bed maintained under isothermal, isobaric, conditions, the molar concentrations in the gas phase at any position and instant of time are obtained by solving the following set of partial differential equations for each of the species *i* in the gas mixture[6, 9, 17]

$$\frac{\partial c_i(t,z)}{\partial t} + \frac{\partial\left(v(t,z)c_i(t,z)\right)}{\partial z} + \frac{\left(1-\varepsilon\right)}{\varepsilon}\rho\frac{\partial \bar{q}_i(t,z)}{\partial t} = 0; \quad i = 1,2,...n \tag{23}$$

In equation (23), t is the time, z is the distance along the adsorber, ρ is the framework density, ε is the bed voidage, v is the interstitial gas velocity, and $\bar{q}_i(t,z)$ is the *spatially averaged* molar loading within the crystallites of radius r_c, monitored at position z, and at time t. The time $t = 0$, corresponds to the time at which the feed mixture is injected at the inlet to the fixed bed. Prior to injection of the feed, it is assumed that an inert, non-adsorbing, gas flows through the fixed bed.

At any time t, during the transient approach to thermodynamic equilibrium, the spatially averaged molar loading within the crystallite r_c is obtained by integration of the radial loading profile

$$\bar{q}_i(t) = \frac{3}{r_c^3}\int_0^{r_c} q_i(r,t)r^2 dr \tag{24}$$

For transient uptake within a crystal at any position and time with the fixed bed, the radial distribution of molar loadings, q_i, within a spherical crystallite, of radius r_c, is obtained from a solution of a set of differential equations describing the uptake

$$\frac{\partial q_i(r,t)}{\partial t} = -\frac{1}{\rho}\frac{1}{r^2}\frac{\partial}{\partial r}\left(r^2 N_i\right) \tag{25}$$

Summing equation (**24**) over all *n* species in the mixture allows calculation of the *total average* molar loading of the mixture within the crystallite

$$\bar{q}_t(t,z) = \sum_{i=1}^{n} \bar{q}_i(t,z) \tag{26}$$

The *interstitial* gas velocity is related to the *superficial* gas velocity by

$$v = \frac{u}{\varepsilon} \tag{27}$$

The adsorber bed is assumed to be initially free of adsorbates, i.e. we have the initial condition

$$t = 0; \quad q_i(0,z) = 0 \tag{28}$$

Equation (28) is relevant to the operation of the transient breakthrough experiments on a laboratory scale, but are not truly reflective of industrial operations.

At time, t = 0, the inlet to the adsorber, z = 0, is subjected to a step input of the *n*-component gas mixture and this step input is maintained till the end of the adsorption cycle when steady-state conditions are reached.

$$t \geq 0; \quad p_i(0,t) = p_{i0}; \quad u(0,t) = u_0 \tag{29}$$

where $u_0 = v_0\varepsilon$ is the superficial gas velocity at the inlet to the adsorber.

The molar loadings at the *outer surface* of the crystallites, i.e. at $r = r_c$, are calculated on the basis of adsorption equilibrium with the bulk gas phase partial pressures p_i at that position z and time t. The adsorption equilibrium can be calculated on the basis of the IAST, or mixed-gas Langmuir, description of mixture adsorption equilibrium, as appropriate.

For convenience, the set of equations describing the fixed bed adsorber are summarized in Figure 2. Typically, the adsorber length is divided into 100 slices, and each spherical crystallite was discretized

into 20 equi-volume slices. The results thus obtained were confirmed to be of adequate accuracy. Combination of the discretized partial differential equations (PDEs) along with the algebraic IAST or RAST equilibrium model, results in a set of differential-algebraic equations (DAEs), which are solved using BESIRK.[12] BESIRK is a sparse matrix solver, based on the semi-implicit Runge-Kutta method originally developed by Michelsen,[13] and extended with the Bulirsch-Stoer extrapolation method.[14] Use of BESIRK improves the numerical solution efficiency in solving the set of DAEs. The evaluation of the sparse Jacobian required in the numerical algorithm is largely based on analytic expressions.[6] Further details of the numerical procedures used in this work, are provided by Krishna and co-workers;[6, 9-11] interested readers are referred to our website that contains the numerical details.[9]

For presenting the breakthrough simulation results, we use the dimensionless time, $\tau = \frac{tu}{L\varepsilon}$, obtained by dividing the actual time, t, by the characteristic time, $\frac{L\varepsilon}{u}$, where L is the length of adsorber, u is the superficial fluid velocity, ε is the bed voidage.[18]

For all the simulations reported in this article we choose the following: adsorber length, L = 0.3 m; cross-sectional area, A = 1 m^2; superficial gas velocity in the bed, u_0 = 0.04 m s^{-1}; voidage of the packed bed, ε = 0.4. Also, the total pressures is assumed to be constant along the length of the fixed bed. Please note that since the superficial gas velocity is specified, the specification of the cross-sectional area of the tube, A, is not relevant in the simulation results presented. The total volume of the bed is $V_{bed} = LA$. The volume of zeolite or MOF used in the simulations is $V_{ads} = LA(1-\varepsilon)$ = 0.18 m^3. If ρ is the framework density, the mass of the adsorbent in the bed is $m_{ads} = \rho LA(1-\varepsilon)$ kg. It is important to note that the volume of adsorbent, V_{ads}, includes the pore volume of the adsorbent material. In these breakthrough simulations we use the same volume of adsorbent in the breakthrough apparatus, i.e. (1 - ε) A L = 0.18 m^3 = 180 L.

For the transient breakthrough simulations presented in this work, three different scenarios are compared for intra-crystalline diffusion:

(1) Intra-particle diffusion described by the Maxwell-Stefan diffusion equations (17), with inclusion of the thermodynamic coupling effects, quantified by $\begin{bmatrix} \Gamma_{11} & \Gamma_{12} \\ \Gamma_{21} & \Gamma_{22} \end{bmatrix}$ for binary mixtures. For these calculations, the use of Equation (12) is of good accuracy, even though the adsorption equilibrium between the bulk fluid phase requires the IAST (or RAST, if thermodynamic non-idealities are important) in many cases.

To demonstrate the importance of thermodynamic coupling on transient breakthroughs, we also perform simulations in which the matrix of thermodynamic factors is taken to be the identity matrix [I], with elements δ_{ik}, the Kronecker delta. Equation (19) is used to describe the transfer fluxes.

(2) In this scenario we assume that the values of $\frac{Đ_i}{r_c^2}$ are large enough to ensure that intra-crystalline gradients are absent and the entire crystallite particle can be considered to be in thermodynamic equilibrium with the surrounding bulk gas phase at that time *t*, and position *z* of the adsorber:

$$\bar{q}_i(t,z) = q_i(t,z) \tag{30}$$

Use of Equation (30) is termed the "no diffusion" scenario.

6. Transient CO_2/C_2H_6 mixture uptake in DDR zeolite

DDR zeolite consists of cages, of 278 Å^3 size, separated by narrow windows.[1, 19] Correlation effects are considered to be negligible, and we use equation (17). Binder et al.[20] and Lauerer et al.[21] report a set of three mixture uptake experiments with 1:1, 2:1, and 3:1 partial pressure ratios for CO_2 and C_2H_6 in the gas phase.

We simulate the three set of experiments reported by Binder/Lauerer.[20, 21]

Experiment 1: 1:1 $CO_2(1)/C_2H_6(2)$ bulk gas mixture at 298 K, p_1 = 20 kPa, p_2 = 20 kPa.

Experiment 2: 2:1 $CO_2(1)/C_2H_6(2)$ bulk gas mixture at 298 K, p_1 = 40 kPa, p_2 = 20 kPa.

Experiment 3: 3:1 $CO_2(1)/C_2H_6(2)$ bulk gas mixture at 298 K, p_1 = 60 kPa, p_2 = 20 kPa.

The data on the unary isotherms of CO_2 and C_2H_6 at 298 K are provided in Figure 36, Chapter 4 of the PhD dissertation of Binder.[22] The unary isotherms for both CO_2, and C_2H_6 can be described adequately by a single-site Langmuir isotherm

$$q_i = \frac{q_{i,sat} b_i p_i}{1 + b_i p_i} \tag{31}$$

The single-site Langmuir parameters are provided in Table 1.

The diffusivity input values of $Đ_1/r_c^2$, and $Đ_2/r_c^2$ are taken from earlier work[7]:

Experiment 1: $Đ_1/r_c^2 = 0.125$ s^{-1}; $Đ_1/Đ_2 = 1333$.

Experiment 2: $Đ_1/r_c^2 = 9.375\times10^{-3}$ s^{-1}; $Đ_1/Đ_2 = 100$.

Experiment 3: $Đ_1/r_c^2 = 6.25\times10^{-3}$ s^{-1}; $Đ_1/Đ_2 = 50$.

For the uptake simulations, the crystallite radius was taken to be 40 μm.

Using comparisons with IAST calculations, Krishna[7] has established that the mixed-gas Langmuir model predicts the mixture adsorption equilibrium with good accuracy.

Figures **3**a,b,c provides a compilation of experimental data of Binder et al.[20] and Lauerer et al.[21] on the transient spatially-averaged component loadings during transient uptake of CO_2/C_2H_6 in DDR. In their experimental investigations using interference microscopy (IFM), the uptake of CO_2, and C_2H_6 within crystals of DDR zeolite exposed to a bulk gas phase consisting of 1:1, 2:1, and 3:1 CO_2/C_2H_6 mixtures are monitored. In the three sets of experiments, overshoots in CO_2 loadings are observed during transient equilibration; see Figures **3**a,b,c.

The Maxwell-Stefan-Glueckauf model captures the overshoots in CO_2 loadings with good accuracy.

7. Transient CO_2/C_2H_6 mixture permeation across DDR zeolite membrane

Transient overshoots are also experienced for membrane permeation. The transient permeation fluxes are obtained by solving the set of partial differential equations

$$\frac{\partial q_i(z,t)}{\partial t} = -\frac{1}{\rho}\frac{\partial}{\partial z}\left(N_i\right) \tag{32}$$

where z is the distance coordinate along the direction of membrane thickness. The boundary conditions are the partial pressures and component molar loadings at the upstream ($z = 0$) and downstream ($z = \delta$) faces of the membrane.

$$\begin{aligned} z &= 0; \quad p_i = p_{i0}; \quad q_i = q_{i0} \\ z &= \delta; \quad p_i = p_{i\delta}; \quad q_i = q_{i\delta} \end{aligned} \tag{33}$$

Figure 4 presents the simulations for r transient permeation of 1:1 $CO_2(1)/C_2H_6(2)$ gas mixtures across a DDR zeolite membrane of thickness 40 μm, and operating at 298 K and total pressure of 40 kPa in the upstream compartment. The continuous solid lines are simulations using the Maxwell-Stefan diffusion equations (17), with parameters: $Đ_1/r_c^2 = 0.125$ s^{-1}; $Đ_1/Đ_2 = 1333$. The dashed lines are the simulations in which thermodynamic coupling effects are ignored and Equation (19) is used to describe the transfer fluxes. Including, thermodynamic coupling results in transient overshoots in the flux of CO_2; the flux overshoot disappears when the thermodynamic coupling effects are neglected.

8. Separating CO_2/C_2H_6 mixtures in fixed bed adsorber packed with DDR zeolite

The Binder/Lauerer uptake experiments suggest the possibility of diffusion-selective purification of ethane by selective removal of CO_2 present as impurities in mixtures with ethane. The separation of CO_2/C_2H_6 is relevant in the context of natural gas processing. Current technologies for CO_2/C_2H_6 separations use extractive distillation because of CO_2/C_2H_6 azeotrope formation.[23] Another alternative is to combine distillation technology with membrane separations; for this purpose cross-linked polyethylene oxide (XLPEO) membranes have demonstrated to have good separation potential.[24-26]

To demonstrate the concept of diffusion-selective separations, we carried out transient breakthrough simulations in a fixed bed adsorber packed with crystallites of DDR, using the methodology described in above.

Figure 5a shows the transient breakthrough of 1:1 CO_2/C_2H_6 mixtures through fixed bed adsorber packed with DDR crystals operating at 298 K, and total pressure p_t = 100 kPa. The *y*-axis is the gas phase concentration at the adsorber outlet, normalized with respect to the feed concentrations at the inlet. The *x*-axis is the dimensionless time, $\tau = tv/L$, obtained by dividing the actual time, *t*, by the characteristic time, L/v. The continuous solid lines are simulations taking due account of intra-crystalline diffusion using the Maxwell-Stefan diffusion equations (17), with parameters: $Đ_1/r_c^2$ = 0.00125 s^{-1}; $Đ_1/Đ_2$ = 1333.

We note that C_2H_6 breaks through earlier and can be recovered in purified form during the early stages of the transient operations, prior to the breakthrough of CO_2. The dashed lines in Figure 5a are the simulations in which thermodynamic coupling effects are ignored and Equation (19) is used to describe the transfer fluxes. In this scenario, no intra-crystalline overshoots of CO_2 occur within the particle and, consequently, the breakthrough of CO_2 occurs earlier. The net result is the productivity of purified C_2H_6 is significantly lowered.

The breakthrough simulations indicated by the dotted lines in Figure 5b correspond to the scenario in which intra-crystalline diffusion limitations are considered to be of negligible importance, i.e. $Đ_1/r_c^2 \to \infty$; $Đ_2/r_c^2 \to \infty$. In this "equilibrium" scenario, CO_2 breaks through earlier and purified C_2H_6 cannot be produced during the adsorption phase of fixed bed operations.

9. Transient uptake of N_2/CH_4 mixture in LTA-4A zeolite

The Habgood[27] experimental data were measured at 194 K with partial pressures p_1 =50.9 kPa and p_2 =49.1 kPa. The N_2(1)/CH_4(2) mixture constitutes a combination of more-mobile-less-strongly-adsorbed-N_2 and tardier-more-strongly-adsorbed-CH_4. Nitrogen is a "pencil-like" molecule (4.4 Å × 3.3 Å) that can hop length-wise across the narrow windows; the "spherical" CH_4 (3.7 Å) is much more severely constrained and has a diffusivity that is 22 times lower than that of N_2.

Table 2 provides the 1-site Langmuir parameters for N_2 and CH_4 in LTA-4A zeolite at 194 K. N_2 has an adsorption strength that is a factor 2.2 lower than that of CH_4. The mixture adsorption equilibrium is described perfectly by the mixed-gas Langmuir equation (11).

The parameter values used in the simulations are: $Đ_1/r_c^2 = 1.56\times10^{-5}$ s^{-1}; $Đ_2/r_c^2 = 7.2\times10^{-9}$ s^{-1}. These are taken from earlier work.[7]

Figure 6 presents a comparison of the experimental data of Habgood[27] on transient uptake of $N_2(1)/CH_4(2)$ mixture within LTA-4A crystals, with simulations of transient uptake with three different scenarios. The Maxwell-Stefan-Glueckauf model captures the overshoots in N_2 loadings with good accuracy.

10. Separating N_2/CH_4 mixtures in in fixed bed adsorber packed with LTA-4A zeolite

In order to demonstrate the importance of proper modeling of intra-crystalline fluxes on separations of $N_2(1)/CH_4(2)$ mixtures using LTA-4A zeolite, Figures 7a,b compares the transient breakthrough results with three different scenarios for calculations of the intra-crystalline diffusion fluxes. Figure

The continuous solid lines in Figures 7a,b are simulations taking due account of intra-crystalline diffusion using the Maxwell-Stefan diffusion equations (17), with parameters: $Đ_1/r_c^2 = 1.56\times10^{-5}$ s^{-1}; $Đ_2/r_c^2 = 7.2\times10^{-9}$ s^{-1}. During the time interval between the breakthroughs of CH_4 and N_2, purified CH_4 can be recovered. The dashed lines in Figure 7a represent simulations in which thermodynamic coupling effects are ignored and Equation (19) is used to describe the transfer fluxes. Ignoring thermodynamic coupling has the effect of significantly reducing the time interval between the breakthroughs of CH_4 and N_2; consequently, there is a significant reduction in the amount of purified CH_4 that can be recovered.

The dotted lines in Figure 7b are simulations in which intra-crystalline diffusion limitations are considered to be of negligible importance, i.e. $Đ_1/r_c^2 \to \infty$; $Đ_2/r_c^2 \to \infty$. In this "equilibrium" scenario, N_2 breaks through earlier and purified CH_4 cannot be produced during the adsorption phase of fixed bed operations.

11. Transient uptake of nC6/2MP mixture in MFI zeolite

The transient uptake of *n*-hexane(nC6)/2-methylpentane(2MP) mixtures in microporous crystals of MFI zeolite, exposed to an equimolar gas phase mixture at constant total pressure (= 2.6 Pa) have been reported by Titze et al.[28] The transient equilibration of nC6 displays a pronounced overshoot, achieving supra-equilibrium loadings during transient equilibration. Titze et al.[28] have established the validity of the M-S equations (17) to model intra-crystalline fluxes by detailed consideration of correlation effects. The mixture adsorption equilibrium is determined using the IAST; the unary isotherm data are provided in Table 3. The input data on diffusivities are: $Đ_1/r_c^2 = 0.016$ s^{-1}; $Đ_2/r_c^2 = 1.6\times10^{-4}$ s^{-1}; These are taken from earlier work.[28]

12. Transient uptake of ethanol/1-propanol mixtures in SAPO-34

The experimental data of Saint-Remi et al.[29] for transient uptake of ethanol/1-propanol mixtures within SAPO-34, that is the structural analog of CHA zeolite, are shown in Figure 8a. The more mobile ethanol is found to exhibit a pronounced maximum in the uptake transience.

In order to rationalize the experimental observations, let us examine the data on the pure component isotherms for ethanol and 1-propanol in CHA, which is a cage type zeolite that consists of 316 Å^3 sized cages separated by 3.8 Å × 4.2 Å sized windows. Configurational-Bias Monte Carlo (CBMC) simulations of unary isotherms in CHA at 300 K, as reported in the work of Krishna and van Baten,[30] are shown in Figure **9**a. The continuous solid lines in Figure **9**a are fits using the dual-site Langmuir-Freundlich model with parameters as specified in Table 4. Figure **9**b presents snapshots of the location, and conformations, of the 1-alcohols within the cages of CHA at saturation conditions.

The CBMC simulations for ethanol/1-propanol mixtures are shown in Figure **9**c. For total fluid phase fugacities, $f_t < 300$ kPa, the adsorption selectivity is strongly in favor of the longer 1-propanol molecule. However, when the total fluid phase fugacity f_t exceeds 600 kPa, we find a reversal of selectivity. This selectivity reversal is entropy-based and is ascribable to the significantly higher saturation capacity of ethanol (4 molecules per cage) in comparison to that of 1-propanol (2 molecules per cage).

The IAST estimations (shown by the dashed lines in Figure **9**c) provide good, quantitative, description of mixture adsorption. In particular, the selectivity reversal phenomenon is properly captured by the IAST.

Transient uptake simulations, using a combination of the Maxwell-Stefan and Glueckauf models can be used to model the transient uptake of ethanol/1-propanol mixtures within CHA crystals. The approach we adopt is to "fit" the values of the Maxwell-Stefan diffusivities to match the experimental data of Saint-Remi et al.[29] The values of the fit parameters are $Đ_{ethanol}/r_c^2 = 3\times10^{-5}$ s^{-1}; $Đ_{1-propanol}/r_c^2 = 1\times10^{-7}$ s^{-1}, were chosen to match the experimental uptakes. The partial fugacities in the bulk fluid mixture are taken to be $f_{ethanol} = f_{1\text{-propanol}} = 150$ kPa. The continuous solid lines in Figure 8a are transient uptake simulations using the Maxwell-Stefan-Gluekauf model. The dashed lines are the calculations using uncoupled flux equation (**19**), together with the classic Glueckauf model; in this scenario, no ethanol overshoot is detected.

Remy et al.[31] report data transient breakthroughs of ethanol/1-propanol and ethanol/1-hexanol mixtures in a fixed bed adsorber packed with SAPO-34, that has the same structural topology as CHA zeolite; see Figure 10a,b. The experiments show that the component that is eluted first from the adsorber is the alcohol with the longer chain length. In other words, the separations are not dictated by the binding strengths in the Henry regime. Rather, the breakthroughs confirm the selectivity reversal phenomena and preferential adsorption of the shorter 1-alcohol. The proper modeling of the breakthrough experiments of Remy et al.[31] requires the inclusion of thermodynamic coupling effects in the diffusion formulation, as has been demonstrated by Krishna.[7]

13. Transient uptake of n-C_4H_{10}/iso-C_4H_{10} in MFI zeolite

Figure 11 presents simulations of the transient uptake of 1/9 n-butane(nC4)/iso-butane(iC4) mixtures in MFI. The linear *n*-butane has a mobility that is about 1-2 orders of magnitude higher than that of the branched isomer because of subtle configurational differences; this has been established PFG NMR experiments of Fernandez et al.[32] Configurational-entropy effects also serve to prefer the adsorption of

the linear isomer.[28] The continuous black solid lines in Figure 11 are simulation results for the Maxwell-Stefan-Glueckauf model. The continuous red solid lines are the calculations using the Maxwell-Stefan-Geddes model. The dotted blue lines are the exact numerical solutions, as presented in earlier work.[7] The Maxwell-Stefan-Glueckauf model is seen to be of adequate accuracy.

14. Separations of O_2/N_2 mixtures; some general remarks

The separation of air to produce N_2 and O_2 of high purities is one of the most important industrial processes that uses pressure swing adsorption technology.[33, 34] The process technologies are geared to either production of purified O_2 or purified N_2. Cryogenic distillation has been the common technologies for this separation, but adsorptive separations offer energy efficient alternatives. Purified O_2 is required for a wide variety of applications that include portable adsorption units for medical applications and in space vehicles. Nitrogen is required in applications where it is desired or necessary to exclude oxygen. Typical industrial applications include laser cutting, food packaging, and nitrogen blanketing. N_2 is required for use in laboratory analytical equipment such as GC, LC, LCMS, FTIR, ICP, and in glove boxes.

For production of purified O_2, cation-exchanged zeolites LTA-5A, NaX, CaX, LiX, and LiLSX (= low silica LiX zeolite) and can be used as selective adsorbents.[34-38] The larger permanent quadrupole of N_2 compared to that of O_2 is responsible for the stronger adsorption strength of N_2 on these zeolites.[37] Both O_2, and N_2 have similar polarizabilities and magnetic susceptibilies. However, the quadrupole moment of N_2 is about 4 times that of O_2.

For production of pure N_2 from air, a different strategy is often employed that rely on diffusion selectivity.[39, 40] Diffusion-selective separation are achieved with Carbon Molecular Sieve (CMS), and LTA-4A zeolite. Diffusion limitations manifest in LTA-4A because the window regions are partially blocked by the cations (see pore landscape in Figure 12).

15. Transient uptake of O_2/N_2 mixtures in LTA-4A

Figure 12 presents the simulations of transient uptake of $O_2(1)/N_2(2)$ mixture in LTA-4A zeolite at 298 K and total pressure of 200 kPa. The partial pressures of the components in the bulk gas phase are p_1 = 42 kPa, p_2 = 158 kPa. The continuous solid lines are the Maxwell-Stefan-Glueckauf model calculations using the input parameters: $Đ_1/r_c^2 = 2\times10^{-3}$ s^{-1}; $Đ_1/Đ_2 = 100$. The dotted lines are exact numerical solutions of the Maxwell-Stefan diffusion equations (17), using the numerical procedures described in this document. The Maxwell-Stefan-Glueckauf model is seen to be of adequate accuracy.

The O_2 overshoot is not very prominent; this is because the differences in the Langmuir binding constants differ by only a factor two. Consequently, the tthermodynamic coupling effects, that engender overshoots, are not severe.

16. Transient breakthrough of O_2/N_2 mixtures in fixed bed adsorber packed with LTA-4A

Diffusion-selective separations may be exploited for production of pure N_2 relies on the significantly lower diffusivity of N_2 as compared to O_2. To demonstrate the feasibility of this concept, Figure 13 presents transient breakthrough simulations for a fixed bed operating at 200 kPa and 298 K.The continuous solid lines in Figure 13 are simulations that include diffusional effects with $Đ_{O2}/r_c^2 = 2\times10^{-3}$ s^{-1}; $Đ_{O2}/Đ_{N2} = 100$, including thermodynamic coupling effects.[39, 40] Neglecting thermodynamic coupling effects leads to practically identically breakthrough characteristics; this is because the differences in the adsorption strengths of O_2 and N_2 in LTA-4A are small. N_2 of purity close to 100% can be recovered during the early stages of the breakthrough, albeit for a very brief time interval. The dotted lines are breakthrough simulations in which diffusional influences are ignored, and thermodynamic equilibrium is assumed to prevail within the crystals; in this case, oxygen breaks through earlier and pure nitrogen cannot be produced.

17. Transient uptake of C_3H_6/C_3H_8 mixtures in ZIF-8

ZIF-8 has a cage-window SOD (sodalite) topology (see pore landscape inFigures 14). The crystallographic size of the windows of ZIF-8 are 3.3 Å, but the windows are flexible. Due to subtle differences in bond lengths and bond angles, the diffusivity of C_3H_6 (1) is significantly higher than that of C_3H_8 (2); Li et al.[41] report the value of the ratio $Đ_1/Đ_2$ = 125 based on the data on pure component uptakes. In ZIF-8, the adsorption strength of the saturated propane is higher than that of propene. From the experimental isotherm data of Li et al.,[41] the ratio of single-site Langmuir parameter b_2/b_1 = 1.07 at 303 K. in sizeFrom a practical standpoint, it is of interest to know under what set of conditions transient overshoots can be expect to occur. To get some insights into this question, we investigated binary C_3H_6(1)/C_3H_8(2) mixture uptake in ZIF-8. The windows of ZIF-8 have a dimension of about 3.3 Å. Due to subtle differences in bond lengths and bond angles (see Figures 14), the diffusivity of C_3H_6 is higher than that of C_3H_8;

Figure 14 presents simulations of transient uptake of C_3H_6(1)/C_3H_8(2) mixture within crystals of ZIF-8, taking $Đ_1/Đ_2$ =125. The more mobile propene exhibits a sharp overshoot in the uptake for simulations in which thermodynamic coupling is properly accounted for. If thermodynamic coupling effects are ignored, both C_3H_6, and C_3H_8 display monotonous equilibration characteristics.

18. Transient C_3H_6/C_3H_8 permeation across ZIF-8 membrane

For steady-state C_3H_6/C_3H_8 permeation across ZIF-8 membrane, Pan et al.[42] and Liu et al.[43] report permeation selectivities in the range 30 – 35, strongly favoring the unsaturated alkene. Let us examine the transient membrane permeation characteristics. Figure 15 shows the results for simulation of transient permeation of C_3H_6(1)/C_3H_8(2) mixture across ZIF-8 membrane of thickness δ = 10 μm. The partial pressures in upstream membrane compartment, p_{10} = p_{20} = 50 kPa. The downstream compartment is placed under vacuum, i.e. $p_{1\delta} = p_{2\,\delta} \approx 0$. As in the transient uptake simulations we take $Đ_1/Đ_2$ = 125. The simulation results are presented in terms of the normalized fluxes $N_1/\left(\rho q_{10} Đ_1/\delta\right)$,

and $N_2/(\rho q_{20} Đ_2/\delta)$ in which the loadings at the upstream face are: q_{10} = 1.937 mol kg^{-1}, q_{20} = 2.067 mol kg^{-1}. The continuous solid lines are the calculations using Equation (17). We note an overshoot in the flux of the alkene during early stages of the transience. If thermodynamic coupling effects are neglected, the C_3H_6 flux overshoot disappears; see the dashed lines using uncoupled flux equation (19). These conclusions are precisely analogous to those reached on the basis of the transient uptake simulations presented in Figure 14.

The value of the permeation selectivity at steady-state, S_{perm} = 117 for both scenarios, either including thermodynamic coupling or neglecting thermodynamic coupling.The membrane permeation experiments of Pan et al.[42] and Liu et al.[43] are consistent with the choice $Đ_1/Đ_2 \approx 40$.

19. Transient Kr/Xe uptake in SAPO-34 crystal

Figure 16 presents simulation results, with three different models, for transient uptake of 90/10 Kr (1)/Xe (2) mixture in SAPO-34 crystals at bulk total pressure of 400 kPa, and temperature T = 298 K. The Maxwell-Stefan-Geddes model is seen to be of reasonably good accuracy.

20. Transient KrXe permeation across SAPO-34 membrane

Diffusional coupling effects often lead to unusual phenomena such as overshoots in the flux of the more mobile partners during transient mixture permeation across nanoporous membranes. Geus et al.[44] report experimental data on transient permeation CH_4/nC_4H_{10} mixture across MFI; the flux of the more mobile CH_4 exhibits a pronounced maximum. The origin of this overshoot can be traced to thermodynamic coupling effects, embodied in the thermodynamic correction factors.[7] We now demonstrate the possibility of transient overshoots for Kr(1)/Xe(2) mixture permeation across SAPO-34 membrane.

Figure 17a shows the fluxes for transient permeation of 10/90 Kr (1)/Xe (2) across SAPO-34 membrane of thickness δ = 4.7 μm at upstream total pressure of 400 kPa and temperature T = 298 K in

The important advantage of transient operation is that the Kr/Xe selectivity exceeds the steady-state value by about three orders of magnitude; see Figure 17b.

21. Notation

b_i	Langmuir-Freundlich constant, $Pa^{-\nu}$
$[B]$	matrix of inverse M-S coefficients, defined by eq. (13)
$Đ_i$	Maxwell-Stefan diffusivity for molecule-wall interaction, $m^2\ s^{-1}$
$Đ_{ij}$	M-S exchange coefficient for *n*-component mixture, $m^2\ s^{-1}$
$Đ_{12}$	M-S exchange coefficient for binary mixture, $m^2\ s^{-1}$
$[D]$	matrix of Fick diffusivities, $m^2\ s^{-1}$
f_i	partial fugacity of species *i*, Pa
n	number of species in the mixture, dimensionless
L	length of packed bed adsorber, m
N_i	molar flux of species *i* with respect to framework, mol $m^{-2}\ s^{-1}$
p_i	partial pressure of species *i* in mixture, Pa
p_t	total system pressure, Pa
q_i	component molar loading of species *i*, mol kg^{-1}
$q_{i,sat}$	molar loading of species *i* at saturation, mol kg^{-1}
q_t	total molar loading in mixture, mol kg^{-1}
$\bar{q}_i(t)$	spatial-averaged component uptake of species *i*, mol kg^{-1}
r	radial direction coordinate, m
r_c	radius of crystallite, m
R	gas constant, 8.314 J $mol^{-1}\ K^{-1}$
t	time, s
T	absolute temperature, K
u_i	velocity of motion of adsorbate species *i* with respect to the framework material, m s^{-1}
x_i	mole fraction of species *i* in adsorbed phase, dimensionless
z	distance coordinate, m

Greek letters

Γ_{ij}	thermodynamic factors, dimensionless
$[\Gamma]$	matrix of thermodynamic factors, dimensionless
δ	thickness of membrane, m
δ_{ij}	Kronecker delta, dimensionless
ε	voidage of packed bed, dimensionless
η	dimensionless distance, dimensionless
θ_i	fractional occupancy of component *i*, dimensionless
θ_t	fractional occupancy of adsorbed mixture, dimensionless
θ_V	fractional vacancy, dimensionless
Θ_i	loading of species *i*, molecules per unit cage, or per unit cell
$\Theta_{i,sat}$	saturation loading of species *i*, molecules per unit cage, or per unit cell
Θ_t	total mixture loading, molecules per unit cage, or per unit cell
$[\Lambda]$	matrix of Maxwell-Stefan diffusivities, $m^2\ s^{-1}$
μ_i	molar chemical potential, J mol^{-1}
ρ	framework density, kg m^{-3}
τ	time, dimensionless

Subscripts

i	referring to component *i*
t	referring to total mixture
sat	referring to saturation conditions

Table 1. 1-site Langmuir parameters for CO_2 and C_2H_6 in DDR zeolite at 298 K. These parameters have been fitted from the data scanned from Figure 36, Chapter 4 of the PhD dissertation of Binder.[22]

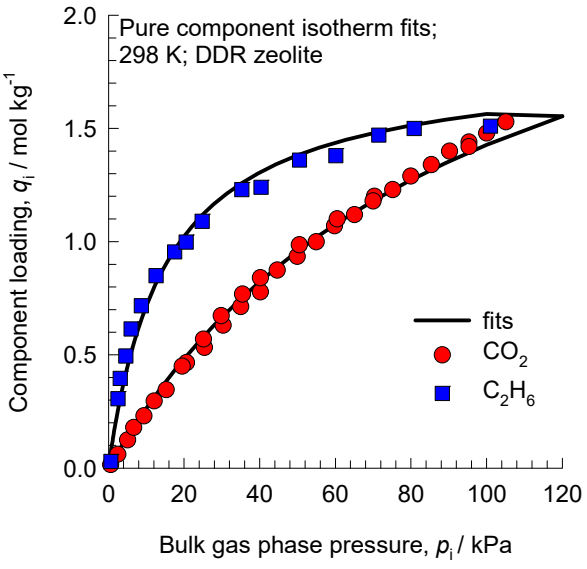

	q_{sat} mol kg^{-1}	b Pa^{-1}
CO_2	2.8	1.04×10^{-5}
C_2H_6	1.8	6.6×10^{-5}

Table 2. 1-site Langmuir parameters for N_2 and CH_4 in LTA-4A zeolite at 194 K. These parameters have been fitted from the isotherm data scanned from the paper by Habgood[27]

	q_{sat} mol kg^{-1}	b Pa^{-1}
N_2	3.6	9.4×10^{-5}
CH_4	3.6	2.08×10^{-4}

Table 3. Dual-site Langmuir-Freundlich parameters for pure component isotherms for hexane isomers in MFI at 298 K. This data is from the Supporting Information of Titze et al.[28] The unary isotherm data are fitted with the dual-Langmuir-Freundlich model

$$\Theta_i = \Theta_{i,A,sat}\frac{b_{i,A}p_i^{\nu_A}}{1+b_{i,A}{}_i^{\nu_A}} + \Theta_{i,B,sat}\frac{b_{i,B}p_i^{\nu_B}}{1+b_{i,B}p_i^{\nu_B}}$$

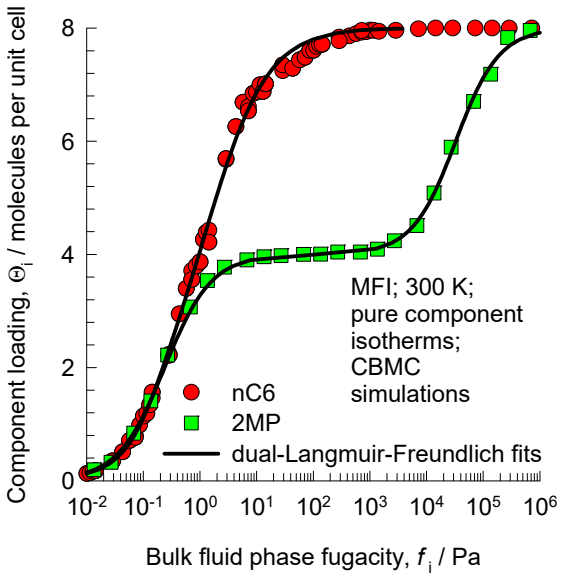

	Site A			Site B		
	$\Theta_{i,A,sat}$ molecules uc^{-1}	$b_{i,A}$ Pa$^{-\nu_i}$	$\nu_{i,A}$ dimensionless	$\Theta_{i,B,sat}$ molecules uc^{-1}	$b_{i,B}$ Pa$^{-\nu_i}$	$\nu_{i,B}$ dimensionless
nC6	6.6	0.7084	0.83	1.4	16.5765	1.5
2MP	4	4.51	1.05	4	7.92×10^{-6}	1.13

Table 4. Dual-site Langmuir-Freundlich parameters for pure component ethanol and 1-propanol in CHA at 300 K. The fit parameters are based on the CBMC simulations of pure component isotherms presented in earlier work.[30] Note that the saturation capacities are specified in molecules per cage; multiply these by 1.387 to obtain the values in mol per kg framework.

	Site A			Site B		
	$\Theta_{i,A,sat}$ Molecules cage^{-1}	$b_{i,A}$ $Pa^{-\nu_i}$	$\nu_{i,A}$ dimensionless	$\Theta_{i,B,sat}$ molecules cage^{-1}	$b_{i,B}$ $Pa^{-\nu_i}$	$\nu_{i,B}$ dimensionless
ethanol	2	7.93×10^{-5}	0.87	2	3.6×10^{-3}	1.14
1-propanol	1	1.28×10^{-2}	1.8	1	9.11×10^{-2}	1

Table 5. Dual-site Langmuir-Freundlich parameters for butane isomers in MFI at 300 K.

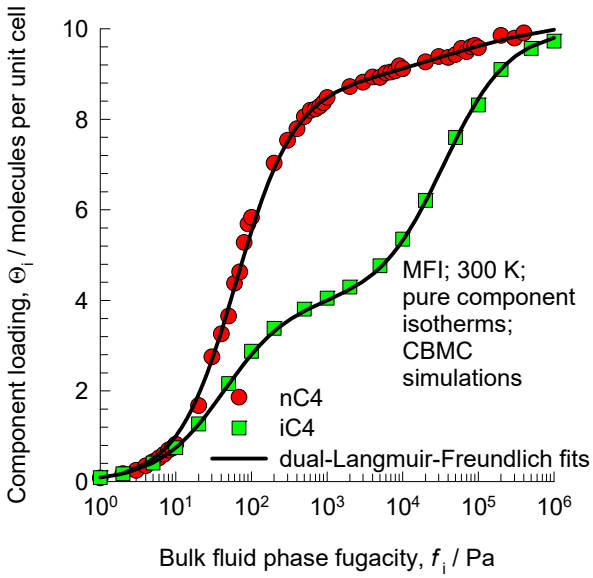

	Site A			Site B		
	$\Theta_{A,sat}$ molecules uc^{-1}	b_A Pa$^{-\nu}$	ν_A dimensionless	$\Theta_{B,sat}$ molecules uc^{-1}	b_B Pa$^{-\nu}$	ν_B dimensionless
nC_4H_{10}	1.5	2.24×10^{-3}	0.57	8.7	9.75×10^{-3}	1.12
iC_4H_{10}	4	2.29×10^{-2}	1	6	2.87×10^{-5}	1

Table 6. 1-site Langmuir parameters for O_2 and N_2 in LTA-4A zeolite at 298 K. These isotherm data are taken from Farooq et al.[39, 40] These data are for RS-10, a modified version of LTA-4A that affords higher diffusion selectivity in favor of O_2.

	q_{sat} mol kg^{-1}	b Pa^{-1}
O_2	1.91	5.65×10^{-7}
N_2	1.91	1.13×10^{-6}

Table 7. 1-site Langmuir parameters for propene and propane in ZIF-8.[45] The *T*-dependent parameters are obtained by fitting the combined sets of pure component isotherm data of Li et al.[41] and Böhme et al.[46] determined for a variety of temperatures in the range 273 K to 408 K.

$$q = q_{sat}\frac{bp}{1+bp}\ ;\ b_A = b_0 \exp\left(\frac{E}{RT}\right)$$

	q_{sat} mol kg^{-1}	b_0 Pa^{-1}	E kJ mol^{-1}
propene	5.2	4.57×10^{-11}	33.9
propane	5.2	1.39×10^{-10}	31.3

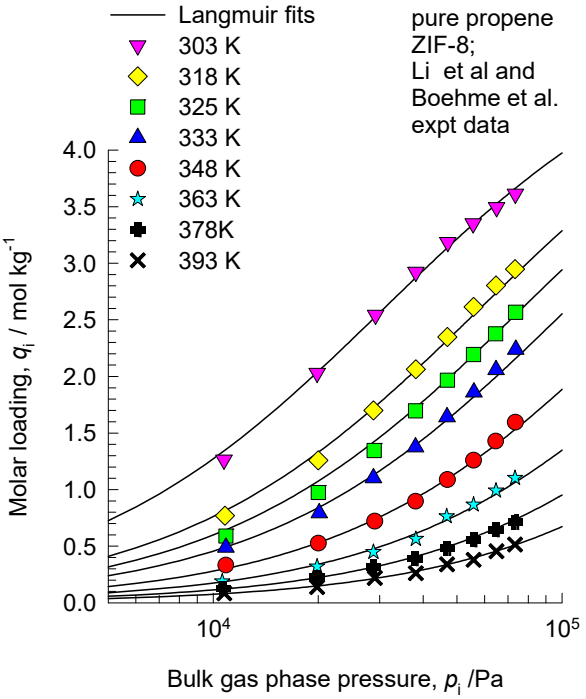

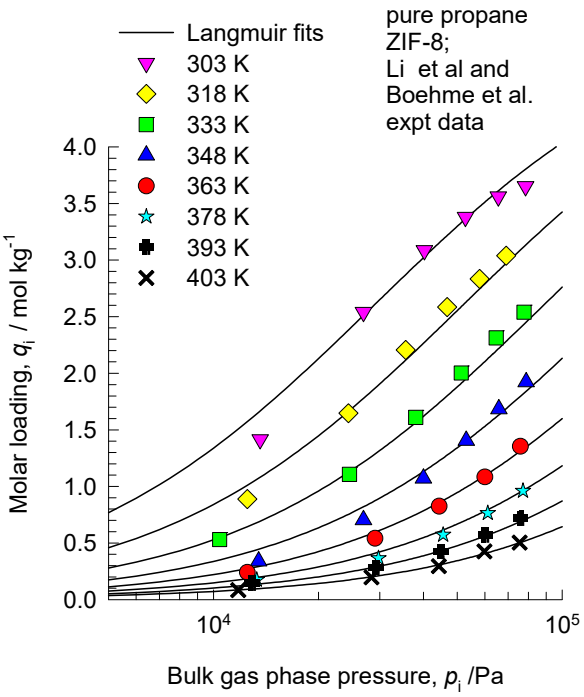

Table 8. *T*-dependent Langmuir parameters for Kr and Xe in SAPO-34. The fit parameters were determined from the unary isotherm data of Kwon et al.[47] measured at temperatures of 308 K, 323 K and 343 K.

	q_{sat} mol kg^{-1}	b_0 Pa^{-1}	E kJ mol^{-1}
Kr	3.1	3.13×10^{-9}	16.3
Xe	3.1	5.52×10^{-9}	19

Table 9. Arrhenius temperature dependence of the M-S diffusivities for Kr and Xe in SAPO-34. The fit parameters were determined the backed-out data for unary and binary permeances as shown below $Đ_i = Đ_{i,0} \exp\left(\frac{-E}{RT}\right)$:

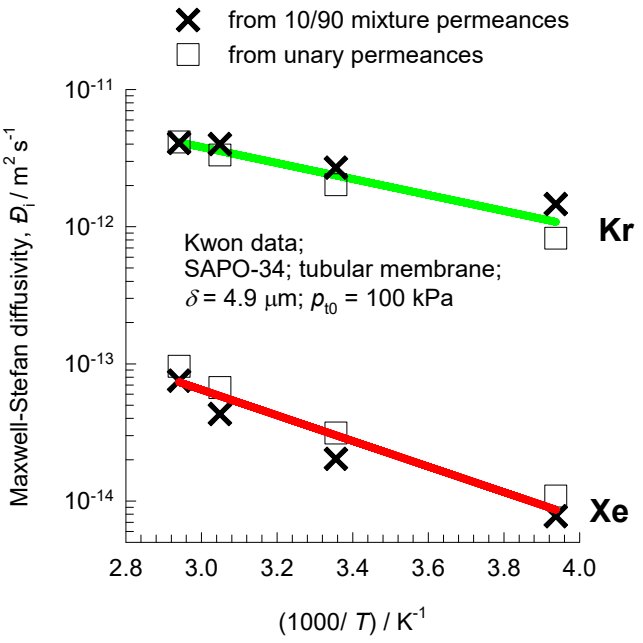

	$Đ_{i,0}$ m^2 s-1	E kJ mol^{-1}
Kr	2.12×10^{-10}	11.14
Xe	4.1×10^{-11}	17.88

22. References

(1) Krishna, R. Diffusion in Porous Crystalline Materials. *Chem. Soc. Rev.* **2012**, *41*, 3099-3118.

(2) Krishna, R. Describing the Diffusion of Guest Molecules inside Porous Structures. *J. Phys. Chem. C* **2009**, *113*, 19756-19781.

(3) Krishna, R.; van Baten, J. M. Onsager coefficients for binary mixture diffusion in nanopores. *Chem. Eng. Sci.* **2008**, *63*, 3120-3140.

(4) Krishna, R.; van Baten, J. M. Investigating the Influence of Diffusional Coupling on Mixture Permeation across Porous Membranes *J. Membr. Sci.* **2013**, *430*, 113-128.

(5) Myers, A. L.; Prausnitz, J. M. Thermodynamics of Mixed Gas Adsorption. *A.I.Ch.E.J.* **1965**, *11*, 121-130.

(6) Krishna, R.; Baur, R. Modelling Issues in Zeolite Based Separation Processes. *Sep. Purif. Technol.* **2003**, *33*, 213-254.

(7) Krishna, R. Tracing the Origins of Transient Overshoots for Binary Mixture Diffusion in Microporous Crystalline Materials. *Phys. Chem. Chem. Phys.* **2016**, *18*, 15482-15495.

(8) Krishna, R.; van Baten, J. M. A molecular dynamics investigation of the diffusion characteristics of cavity-type zeolites with 8-ring windows. *Microporous Mesoporous Mater.* **2011**, *137*, 83-91.

(9) Krishna, R.; Baur, R. Diffusion, Adsorption and Reaction in Zeolites: Modelling and Numerical Issues. http://krishna.amsterchem.com/zeolite/, University of Amsterdam, Amsterdam, 1 January 2015.

(10) Krishna, R.; van Baten, J. M. Investigating the potential of MgMOF-74 membranes for CO_2 capture. *J. Membr. Sci.* **2011**, *377*, 249-260.

(11) He, Y.; Krishna, R.; Chen, B. Metal-Organic Frameworks with Potential for Energy-Efficient Adsorptive Separation of Light Hydrocarbons. *Energy Environ. Sci.* **2012**, *5*, 9107-9120.

(12) Kooijman, H. A.; Taylor, R. A dynamic nonequilibrium model of tray distillation columns. *A.I.Ch.E.J.* **1995**, *41*, 1852-1863.

(13) Michelsen, M. An efficient general purpose method of integration of stiff ordinary differential equations. *A.I.Ch.E.J.* **1976**, *22*, 594-597.

(14) Bulirsch, R.; Stoer, J. Numerical treatment of ordinary differential equations by extrapolation methods. *Numer. Math.* **1966**, *8*, 1-14.

(15) Krishna, R. Screening Metal-Organic Frameworks for Mixture Separations in Fixed-Bed Adsorbers using a Combined Selectivity/Capacity Metric. *RSC Adv.* **2017**, *7*, 35724-35737.

(16) Krishna, R. Methodologies for Evaluation of Metal-Organic Frameworks in Separation Applications. *RSC Adv.* **2015**, *5*, 52269-52295.

(17) Krishna, R. The Maxwell-Stefan Description of Mixture Diffusion in Nanoporous Crystalline Materials. *Microporous Mesoporous Mater.* **2014**, *185*, 30-50.

(18) Krishna, R.; Long, J. R. Screening metal-organic frameworks by analysis of transient breakthrough of gas mixtures in a fixed bed adsorber. *J. Phys. Chem. C* **2011**, *115*, 12941-12950.

(19) Krishna, R.; van Baten, J. M. Comment on Comparative Molecular Simulation Study of CO_2/N_2 and CH_4/N_2 Separation in Zeolites and Metal-Organic Frameworks. *Langmuir* **2010**, *26*, 2975-2978.

(20) Binder, T.; Lauerer, A.; Chmelik, C.; Haase, J.; Kärger, J.; Ruthven, D. M. Micro-imaging of transient intracrystalline concentration profiles during two-component uptake of light hydrocarbon - carbon dioxide mixtures by DDR-type zeolites. *Ind. Eng. Chem. Res.* **2015**, *54*, 8997-9004.

(21) Lauerer, A.; Binder, T.; Chmelik, C.; Miersemann, E.; Haase, J.; Ruthven, D. M.; Kärger, J. Uphill Diffusion and Overshooting in the Adsorption of Binary Mixtures in Nanoporous Solids. *Nat. Commun.* **2015**, *6*, 7697. http://dx.doi.org/doi:10.1038/ncomms8697.

(22) Binder, T. *Mass Transport in Nanoporous Materials: New Insights from Micro-Imaging by Interference Microscopy*. Ph.D. Dissertation, Universität Leipzig, Leipzig, 2013.

(23) Lastari, F.; Pareek, V.; Trebble, M.; Tade, M. O.; Chinn, D.; Tsai, N. C.; Chan, K. I. Extractive Distillation for CO_2–Ethane Azeotrope Separation. *Chem. Eng. Process.* **2012**, *52*, 155-161.

(24) Ribeiro, C. P.; Freeman, B. D.; Paul, D. R. Pure- and Mixed-Gas Carbon Dioxide/Ethane Permeability and Diffusivity in a Cross-linked Poly(ethylene oxide) Copolymer. *J. Membr. Sci.* **2011**, *377*, 110-123.

(25) Krishna, R. Describing Mixture Permeation across Polymeric Membranes by a Combination of Maxwell-Stefan and Flory-Huggins Models. *Polymer* **2016**, *103*, 124-131.

(26) Krishna, R. Using the Maxwell-Stefan formulation for Highlighting the Influence of Interspecies (1-2) Friction on Binary Mixture Permeation across Microporous and Polymeric Membranes. *J. Membr. Sci.* **2017**, *540*, 261-276.

(27) Habgood, H. W. The Kinetics of Molecular Sieve Action. Sorption of Nitrogen-Methane Mixtures by Linde Molecular Sieve 4A. *Canad. J. Chem.* **1958**, *36*, 1384-1397.

(28) Titze, T.; Chmelik, C.; Kärger, J.; van Baten, J. M.; Krishna, R. Uncommon Synergy Between Adsorption and Diffusion of Hexane Isomer Mixtures in MFI Zeolite Induced by Configurational Entropy Effects *J. Phys. Chem. C* **2014**, *118*, 2660-2665.

(29) Saint-Remi, J. C.; Baron, G. V.; Denayer, J. F. M. Non-Uniform Chain Length Dependent Diffusion of Short 1-Alcohols in SAPO-34 in Liquid Phase. *J. Phys. Chem. C* **2013**, *117*, 9758-9765.

(30) Krishna, R.; van Baten, J. M. Entropy-based Separation of Linear Chain Molecules by Exploiting Differences in the Saturation Capacities in Cage-type Zeolites. *Sep. Purif. Technol.* **2011**, *76*, 325-330.

(31) Remy, T.; Saint-Remi, J. C.; Singh, R.; Webley, P. A.; Baron, G. V.; Denayer, J. F. M. Adsorption and Separation of C1-C8 Alcohols on SAPO-34. *J. Phys. Chem. C* **2011**, *115*, 8117-8125.

(32) Fernandez, M.; Kärger, J.; Freude, D.; Pampel, A.; van Baten, J. M.; Krishna, R. Mixture Diffusion in Zeolites Studied by MAS PFG NMR and Molecular Simulation. *Microporous Mesoporous Mater.* **2007**, *105*, 124-131.

(33) Ruthven, D. M.; Farooq, S.; Knaebel, K. S. *Pressure swing adsorption*; VCH Publishers: New York, 1994.

(34) Farooq, S.; Ruthven, D. M.; Boniface, H. A. Numerical-Simulation of a Pressure Swing Adsorption Oxygen Unit. *Chem. Eng. Sci.* **1989**, *44*, 2809-2816.

(35) Rama Rao, V.; Farooq, S.; Krantz, W. B. Design of a Two-Step Pulsed Pressure-Swing Adsorption-Based Oxygen Concentrator. *A.I.Ch.E.J.* **2010**, *56*, 354-370.

(36) Rama Rao, V. *Adsorption based portable oxygen concentrator for personal medical applications*. Ph.D. Dissertation, National University of Singapore, Singapore, 2011.

(37) Sircar, S.; Myers, A. L. *Gas Separation by Zeolites, Chapter 22*. Handbook of Zeolite Science and Technology; Edited by S.M. Auerbach, K.A. Carrado and P.K. Dutta, Marcel Dekker: New York, 2003.

(38) Ritter, J. A. Development of Pressure Swing Adsorption Technology for Spaceflight Oxygen Concentrators. http://www.dsls.usra.edu/meetings/hrp2010/pdf/Friday/Ritter.pdf, NASA Human Research Program, Houston, 2010.

(39) Farooq, S.; Rathor, M. N.; Hidajat, K. A Predictive Model for a Kinetically Controlled Pressure Swing Adsorption Separation Process. *Chem. Eng. Sci.* **1993**, *48*, 4129-4141.

(40) Farooq, S. Sorption and Diffusion of Oxygen and Nitrogen in Molecular- Sieve RS-10. *Gas Sep. Purif.* **1995**, *9*, 205-212.

(41) Li, K.; Olson, D. H.; Seidel, J.; Emge, T. J.; Gong, H.; Zeng, H.; Li, J. Zeolitic Imidazolate Frameworks for Kinetic Separation of Propane and Propene. *J. Am. Chem. Soc.* **2009**, *131*, 10368-10369.

(42) Pan, Y.; Li, T.; Lestari, G.; Lai, Z. Effective Separation of Propylene/Propane Binary Mixtures by ZIF-8 Membranes. *J. Membr. Sci.* **2012**, *390-391*, 93-98.

(43) Liu, D.; Ma, X.; Xi, H.; Lin, Y. S. Gas transport properties and propylene/propane separation characteristics of ZIF-8 membranes. *J. Membr. Sci.* **2014**, *451*, 85-93.

(44) Geus, E. R.; van Bekkum, H.; Bakker, W. J. W.; Moulijn, J. A. High-temperature Stainless Steel Supported Zeolite (MFI) Membranes: Preparation, Module Construction, and Permeation Experiments. *Microporous Mater.* **1993**, *1*, 131-147.

(45) Krishna, R. Evaluation of Procedures for Estimation of the Isosteric Heat of Adsorption in Microporous Materials. *Chem. Eng. Sci.* **2015**, *123*, 191-196.

(46) Böhme, U.; Barth, B.; Paula, C.; Kuhnt, A.; Schwieger, W.; Mundstock, A.; Caro, J.; Hartmann, M. Ethene/Ethane and Propene/Propane Separation via the Olefin and Paraffin Selective Metal−Organic Framework Adsorbents CPO-27 and ZIF-8. *Langmuir* **2013**, *29*, 8592-8600.

(47) Kwon, Y. H.; Kiang, C.; Benjamin, E.; Crawford, P. r.; Nair, S.; Bhave, R. Krypton-Xenon Separation Properties of SAPO-34 Zeolite Materials and Membranes. *A.I.Ch.E.J.* **2017**, *63*, 761-769.

23. Captions for Figures

Figure 1. Schematic of a packed bed adsorber, showing two different discretization schemes for a single spherical crystallite.

Figure 2. Summary of model equations describing packed bed adsorber, along with discretization scheme.

Figure 3. (a, b, c) Experimental data of Binder et al.[20] and Lauerer et al.[21] (indicated by symbols) for spatial-averaged transient uptake of (a) 1:1 (b) 2:1, and (c) 3:1 $CO_2(1)/C_2H_6(2)$ gas mixtures within crystals of DDR zeolite at 298 K. The dashed lines are the calculations using the classic Glueckauf model. The continuous solid lines are calculations based on the Maxwell-Stefan-Glueckauf model, developed in this work. The dotted lines are the calculations using the exact numerical solutions, as reported in the publication of Krishna.[7]

Figure 4. Transient permeation of 1:1 $CO_2(1)/C_2H_6(2)$ gas mixtures within crystals of DDR zeolite at 298 K and total pressure of 40 kPa in the upstream comparment. The continuous solid lines are simulations using the Maxwell-Stefan diffusion equations (17), with parameters: $Đ_1/r_c^2$ = 0.125 s^{-1}; $Đ_1/Đ_2$ = 1333. The dashed lines are the simulations in which thermodynamic coupling effects are

ignored and Equation (19) is used to describe the transfer fluxes. The Maxwell-Stefan model for membrane permeation is described in detail in earlier works.[7, 17, 26]

Figure 5. (a, b) Transient breakthrough of 1:1 CO_2/C_2H_6 mixtures through fixed bed adsorber packed with DDR crystals operating at 298 K, and total pressure p_t = 40 kPa. The continuous solid lines are simulations using the Maxwell-Stefan diffusion equations (17), with parameters: $Đ_1/r_c^2$ = 0.00125 s^{-1}; $Đ_1/Đ_2$ = 1333. The dashed lines are the simulations in which thermodynamic coupling effects are ignored and Equation (19) is used to describe the transfer fluxes. The dotted lines are simulations in which intra-crystalline diffusion limitations are considered to be of negligible importance, i.e. $Đ_1/r_c^2 \to \infty$; $Đ_2/r_c^2 \to \infty$.

Figure 6. Experimental data of Habgood [27] on transient uptake of $N_2(1)/CH_4(2)$ mixture within LTA-4A crystals, exposed to binary gas mixtures at 194 K and partial pressures p_1 =50.9 kPa; p_2 = 49.1 kPa. The dashed lines are the calculations using the classic Glueckauf model. The continuous solid lines are calculations based on the Maxwell-Stefan-Glueckauf model, developed in this work. The dotted lines are the calculations using the exact numerical solutions, as reported in the publication of Krishna.[7]

Figure 7. (a, b) Transient breakthrough of 1:1 $N_2(1)/CH_4(2)$ mixture in fixed bed adsorber packed with LTA-4A crystals operating at 194 K, and total pressure p_t = 100 kPa. The continuous solid lines are simulations using the Maxwell-Stefan diffusion equations (17), with parameters: $Đ_1/r_c^2$ = 1.56×10^{-5} s^{-1};

$Đ_2/r_c^2$ = 7.2×10^{-9} s^{-1}. The dashed lines are the simulations in which thermodynamic coupling effects are ignored and Equation (19) is used to describe the transfer fluxes. The dotted lines are simulations in which intra-crystalline diffusion limitations are considered to be of negligible importance, i.e. $Đ_1/r_c^2 \to \infty; \quad Đ_2/r_c^2 \to \infty$.

Figure 8. (a) Experimental data of Saint-Remi et al.[29] for transient uptake of ethanol/1-propanol mixtures within SAPO-34, that is the structural analog of CHA zeolite. (b) Comparison of experimental data on transient uptake with simulations using the classical Glueckauf (dashed lines), and Maxwell-Stefan-Glueckauf (continuous solid lines) model calculations.

Figure 9. (a) CBMC simulations[30] of pure component adsorption isotherms for ethanol, and 1-propanol in CHA at 300 K. Table **4** provides the pure component isotherm fit parameters. (b) Snapshots showing the conformations of ethanol, and 1-propanol in CHA at saturation conditions. (c) CBMC mixture simulations for ethanol/1-propanol mixtures in CHA at 300 K. The partial fugacities in the bulk fluid phase are taken to be equal, i.e. f_1=f_2. The dashed lines represent IAST calculations using dual-site Langmuir-Freundlich fits of pure component isotherms; Table 4 provides the pure component isotherm fit parameters. The range of liquid phase operation is indicated by the shaded region; the transition between vapor and liquid bulk phase is determined using the Peng-Robinson equation of state.

Figure 10. (a, b) Transient breakthrough experimental data of Remy et al.[31] for separation of (a) ethanol/1-propanol, and (b) ethanol/1-hexanol mixtures in a fixed bed adsorber packed with SAPO-34.

Figure 11. Transient uptake of nC4/iC4 mixture in MFI at 298 K. The initial partial pressures $p_1 = p_2 =$ 0 Pa; final partial pressures $p_1 = 100$ Pa, $p_2 = 900$ Pa. Input data: $Đ_1/r_c^2 = 0.08$ s^{-1}; $Đ_2/r_c^2 = 4\times10^{-3}$ s^{-1}; these values are taken from earlier work by Krishna.[7] The dashed lines are the calculations using the Maxwell-Stefan-Geddes model. The continuous solid lines are calculations based on the Maxwell-Stefan-Glueckauf model, developed in this work. The dotted lines are the calculations using the exact numerical solutions, as reported in the publication of Krishna.[7] The unary isotherm fit parameters are provided in Table 5. The mixture adsorption equilibrium at the surface of the particle is estimated using IAST.

Figure 12. Transient uptake of $O_2(1)/N_2(2)$ mixture in LTA-4A zeolite at 298 K and total pressure of 200 kPa. The partial pressures of the components in the bulk gas phase are $p_1 = 42$ kPa, $p_2 = 158$ kPa. The continuous solid lines are the Maxwell-Stefan-Glueckauf model calculations using the input parameters: $Đ_1/r_c^2 = 2\times10^{-3}$ s^{-1}; $Đ_1/Đ_2 = 100$. The dotted lines are exact numerical solutions of the Maxwell-Stefan diffusion equations (17), using the numerical procedures described in this document. The Langmuir isotherm parameters are provided in Table 6.

Figure 13. (a) (b) Influence of diffusional limitations on the breakthrough characteristics of $O_2(1)/N_2(2)$ mixture in a fixed bed adsorber packed with LTA-4A operating at a total pressure of 200 kPa and 298 K. The partial pressures of the components in the bulk gas phase at the inlet are p_1 = 42 kPa, p_2 = 158 kPa. The continuous solid lines are simulations include diffusional effects with $Đ_{O2}/r_c^2 = 2\times10^{-3}$ s^{-1}, and $Đ_{O2}/Đ_{N2}$ =100, including thermodynamic coupling effects. The dotted lines are breakthrough simulations in which diffusional influences are ignored, and thermodynamic equilibrium is assumed to prevail within the crystals. The adsorption and diffusion data used here are for RS-10 that is a modified version of LTA-4A that affords higher diffusion selectivity in favor of O_2; the data are taken from Farooq et al.[39, 40] The Langmuir isotherm parameters are provided in Table 6.

Figure 14. Simulations of transient uptake of $C_3H_6(1)/C_3H_8(2)$ mixtures within crystals of ZIF-8 at 303 K. The simulations use the isotherm parameters specified in Table **7**, along with $Đ_1/r_c^2 = 1.5\times10^{-2}$ s^{-1}; $Đ_2/r_c^2 = 1.2\times10^{-4}$ s^{-1}; $Đ_1/Đ_2 = 125$; ratio of single-site Langmuir parameter $b_2/b_1 = 1.07$. The continuous solid lines are calculations based on the Maxwell-Stefan-Glueckauf model, developed in this work. The dashed lines are the calculations using the Maxwell-Stefan-Geddes model. The dotted lines are the calculations using the exact numerical solutions, as reported in the publication of Krishna.[7]

Figure 15. Simulation of transient permeation of $C_3H_6(1)/C_3H_8(2)$ mixture across ZIF-8 membrane at 303 K. The diffusivity data used are:[41] $\rho Đ_1/\delta = 1.39\times10^{-4}$ kg m^{-2} s^{-1}, $\rho Đ_2/\delta = 1.11\times10^{-6}$ kg m^{-2} s^{-1}; $Đ_1/Đ_2 = 125$; ratio of single-site Langmuir parameter $b_2/b_1 = 1.07$; membrane thickness $\delta = 10$ μm; partial pressures in upstream membrane compartment, $p_{10} = p_{20} = 50$ kPa. The downstream compartment is placed under vacuum, i.e. $p_{1\delta} = p_{2\delta} \approx 0$. The loadings at the upstream face are: q_{10} =

1.937 mol kg^{-1}, q_{20} = 2.067 mol kg^{-1}. The loadings at the downstream face are: $q_{1\delta} = q_{2\,\delta} \approx 0$. The plots show the normalized fluxes $N_1/(\rho q_{10} Đ_1/\delta)$, and $N_2/(\rho q_{20} Đ_2/\delta)$ as a function of the square root of time. The continuous solid lines are the calculations using Equation (17). The dashed lines are the calculations using uncoupled flux equation (19).

Figure 16. Simulations of transient uptake of 90/10 Kr (1)/Xe (2) mixture in SAPO-34 crystals at bulk total pressure of 400 kPa, and temperature T = 298 K. The isotherm data are based on Kwon et al.[47]; see Table 8. The M-S diffusivity values are based on the Arrhenius fits of the $Đ_i$; the fit constants are provided in Table 9. The continuous solid lines are calculations based on the Maxwell-Stefan-Glueckauf model, developed in this work. The dashed lines are the calculations using the Maxwell-Stefan-Geddes model. The dotted lines are the calculations using the exact numerical solutions.

Figure 17. (a) Transient permeation fluxes and (b) permeation selectivities for 10/90 Kr (1)/Xe (2) mixture permeation across SAPO-34 membrane of thickness δ = 4.9 μm at upstream total pressure of 400 kPa, and temperature T = 298 K. The isotherm data are based on Kwon et al.[47]; see Table 8. The M-S diffusivity values are based on the Arrhenius fits of the $Đ_i$; the fit constants are provided in Table 9. Further details of the membrane calculations are provided in our earlier work.[26]

Figure S1

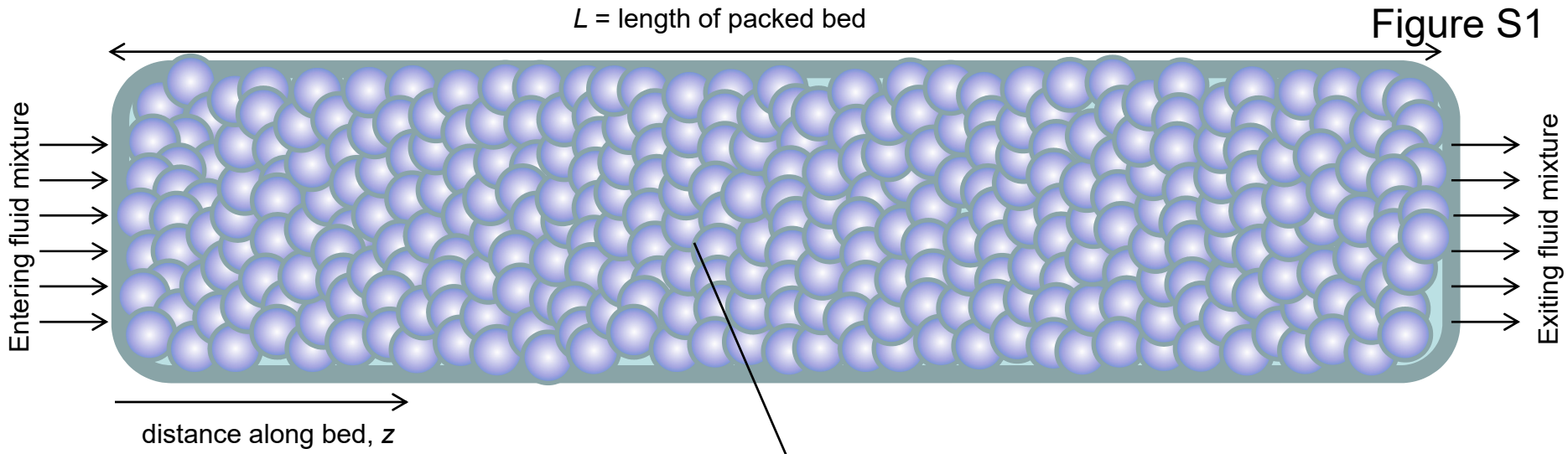

Two different discretization strategies for adsorbent particle

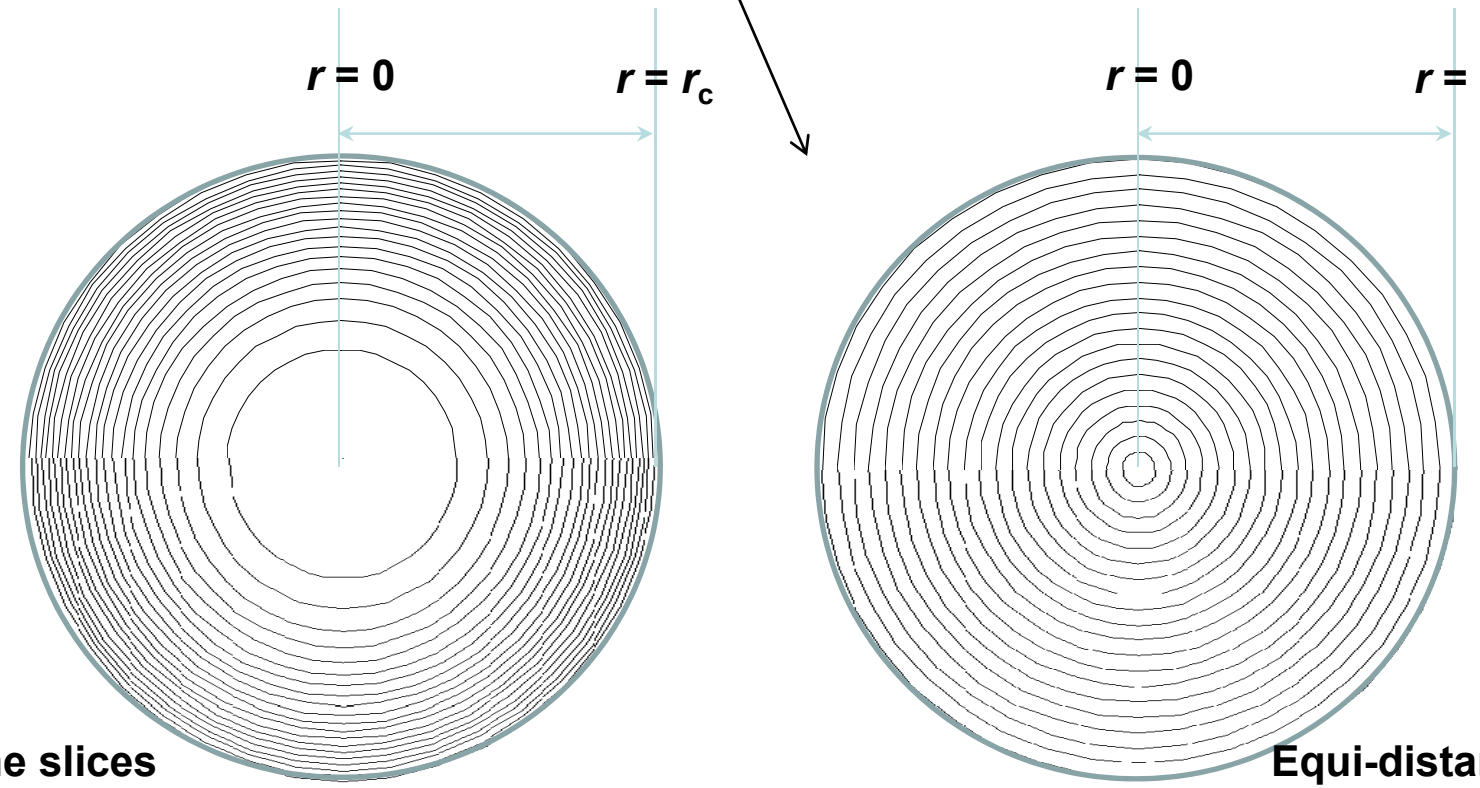

Equi-volume slices

Equi-distant slices

Fixed bed breakthrough model

Figure S2

Component balance

$$\frac{1}{RT}\frac{\partial p_i}{\partial t} = -\frac{1}{RT}\frac{\partial (v p_i)}{\partial z} - \frac{(1-\varepsilon)}{\varepsilon}\rho\frac{\partial \bar{q}_i}{\partial t}; \quad i = 1,2,...n$$

Balance for mixture

$$\frac{1}{RT}p_t\frac{\partial (v(t,z))}{\partial z} = -\frac{(1-\varepsilon)}{\varepsilon}\rho\frac{\partial \bar{q}_t(t,z)}{\partial t}$$

Average loading within crystal

$$\bar{q}_i = \frac{3}{r_c^3}\int_0^{r_c} q_i r^2 dr$$

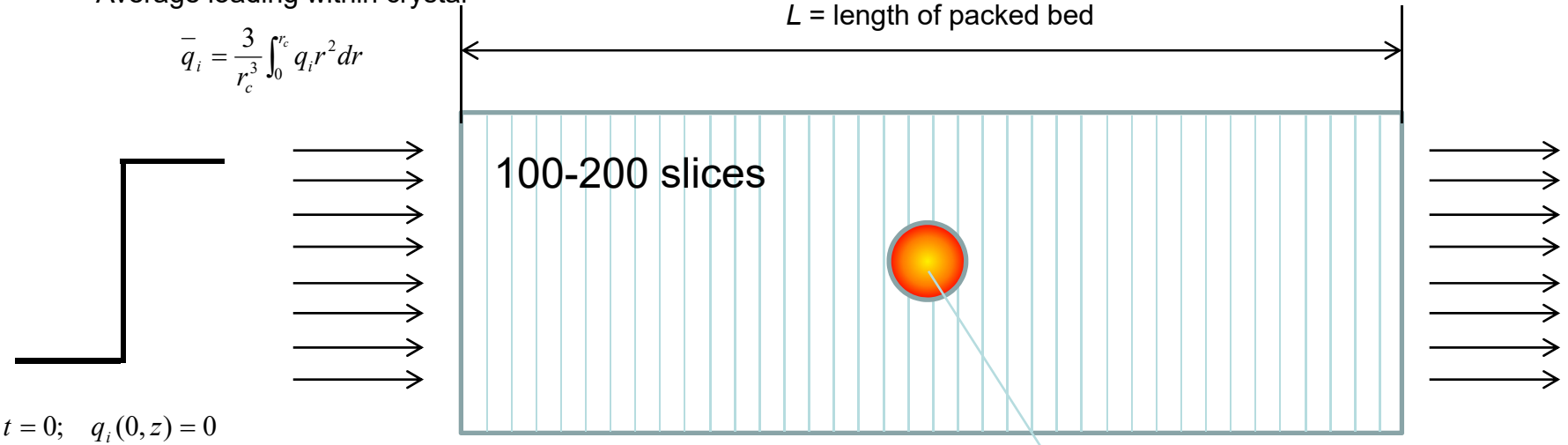

$$t = 0; \quad q_i(0,z) = 0$$

$$t \geq 0; \quad p_i(0,t) = p_{i0}; \quad u(0,t) = u_0$$

Uptake within crystal

$$\frac{\partial q_i}{\partial t} = -\frac{1}{\rho}\frac{1}{r^2}\frac{\partial}{\partial r}\left(r^2 N_i\right)$$

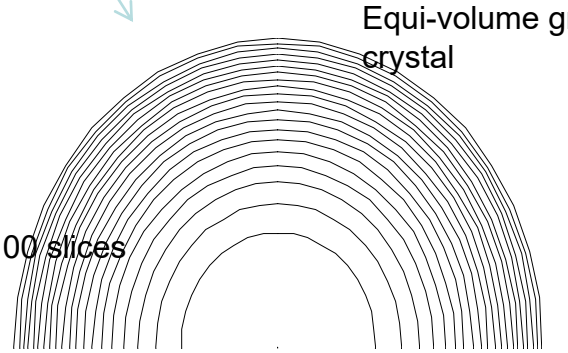

Maxwell-Stefan equations

$$-\rho\frac{q_i}{RT}\nabla\mu_i = \sum_{\substack{j=1 \\ j\neq i}}^{n}\frac{x_j N_i - x_i N_j}{Đ_{ij}} + \frac{N_i}{Đ_i}; \quad i = 1,2,..n$$

Transient CO_2/C_2H_6 uptake in DDR zeolite

Figure S3

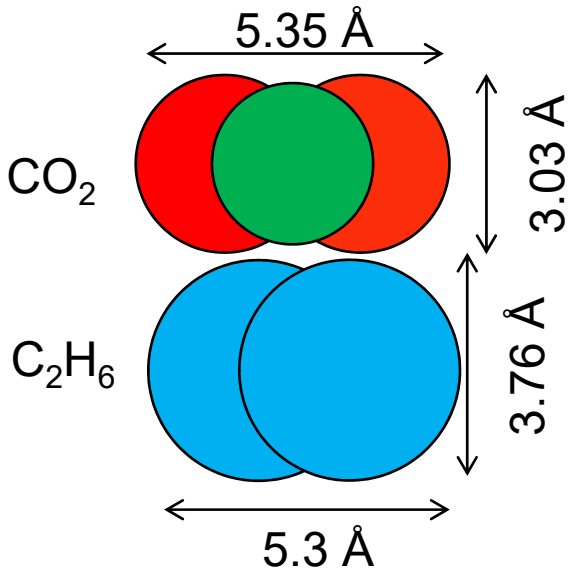

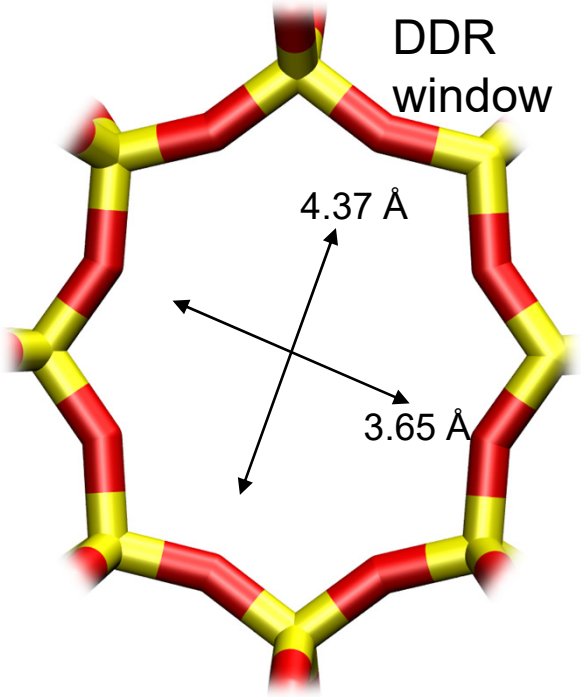

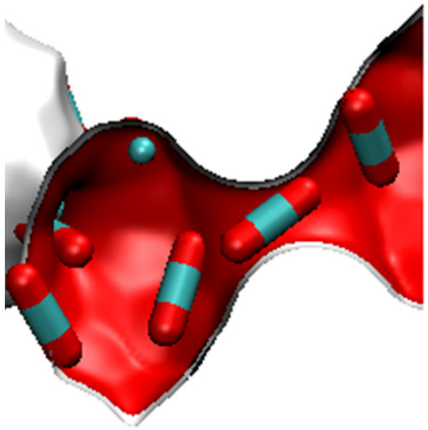

CO_2 hops lengthwise across windows; therefore has a higher diffusivity

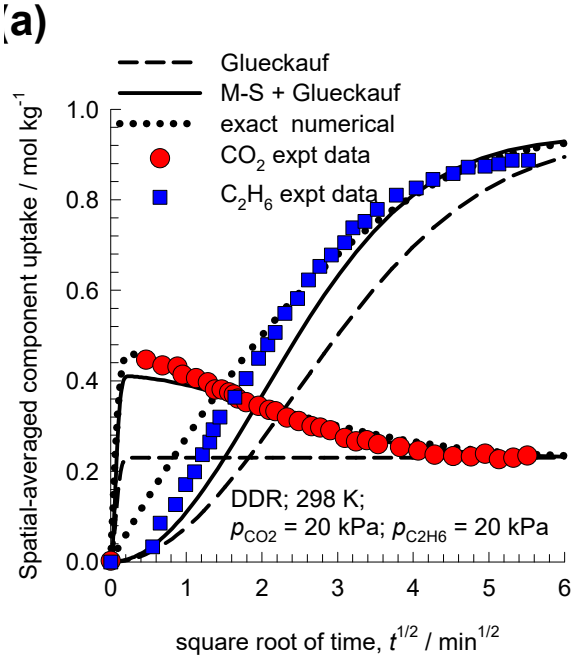

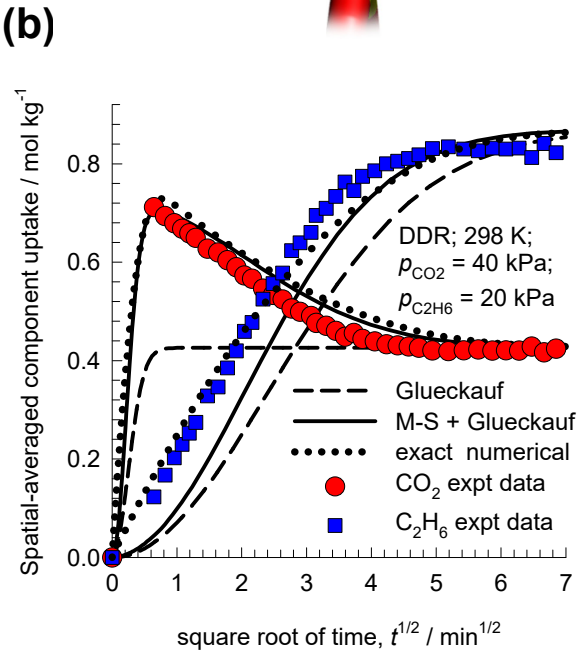

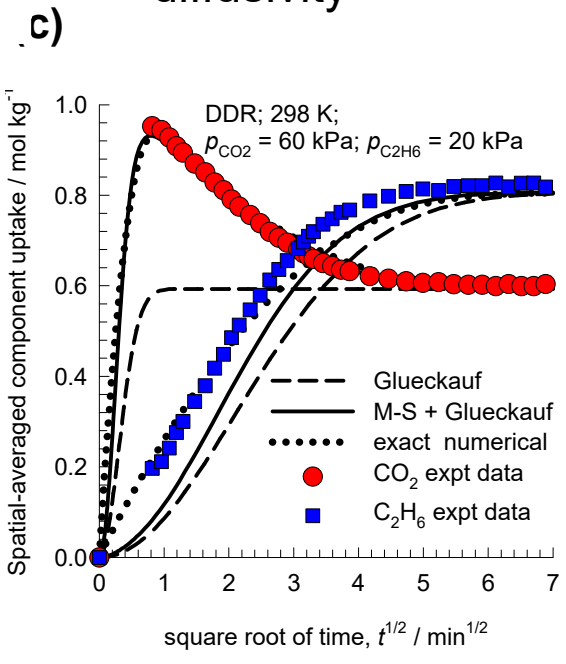

Figure S4

Transient CO_2/C_2H_6 permeation across DDR membrane

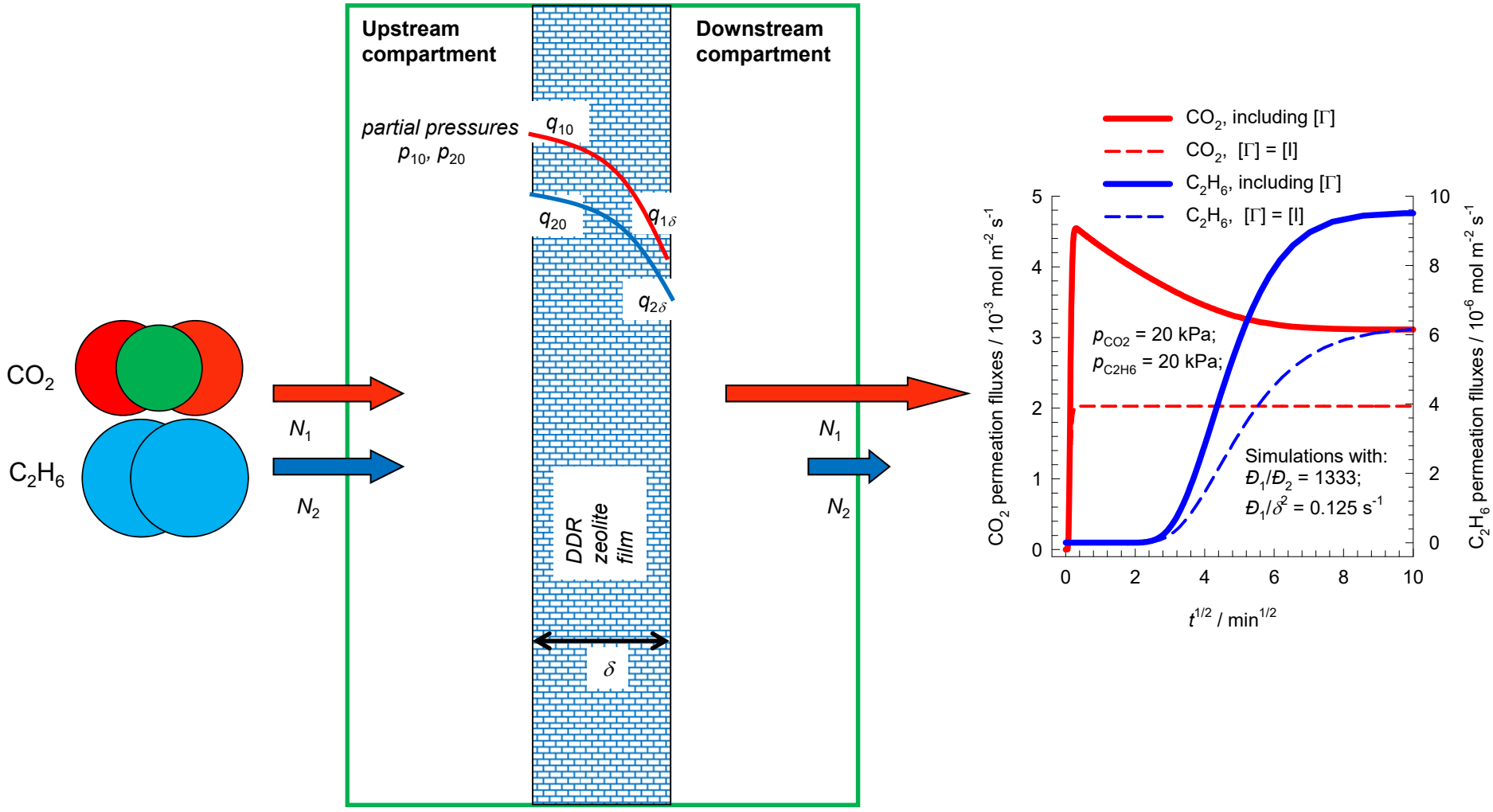

Figure S5

Transient breakthrough in fixed bed with DDR

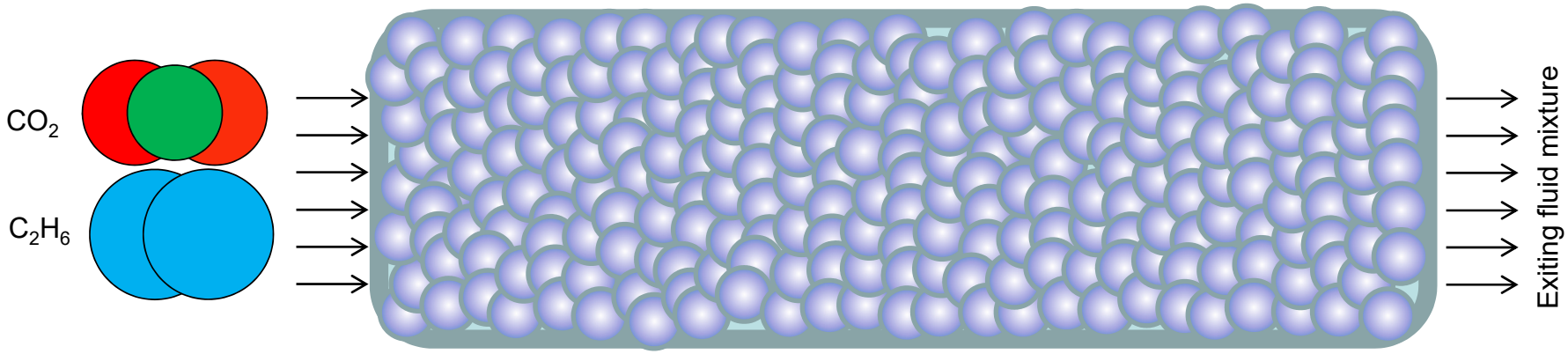

(a)

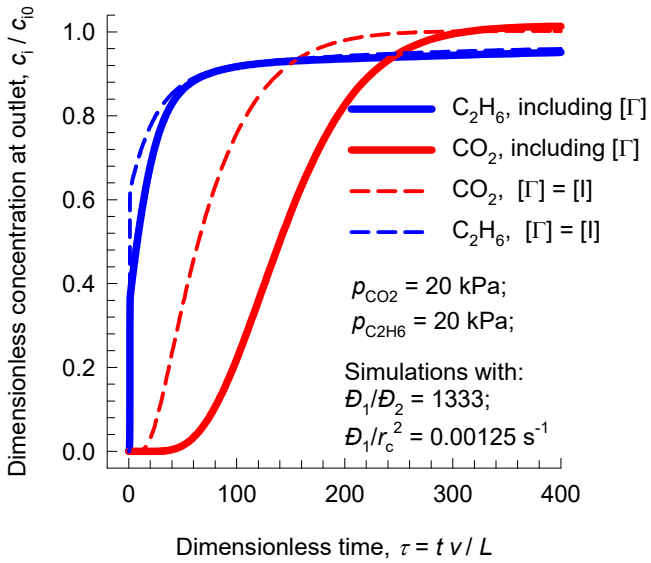

(b)

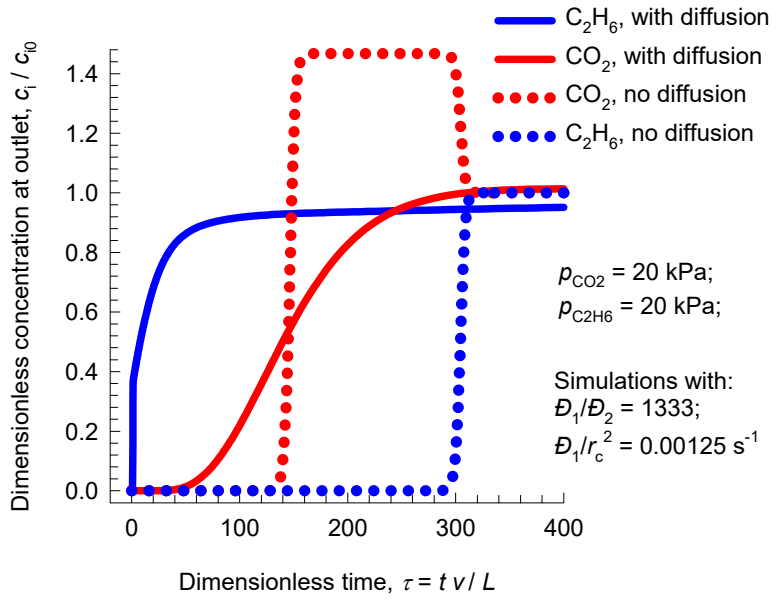

N_2/CH_4 mixture uptake LTA-4A

Figure S6

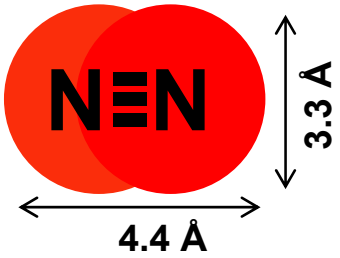

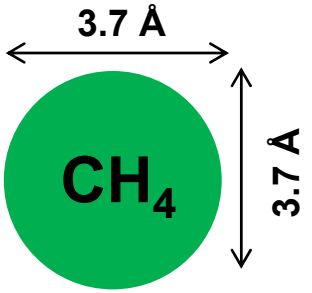

LTA-4A (96 Na+)

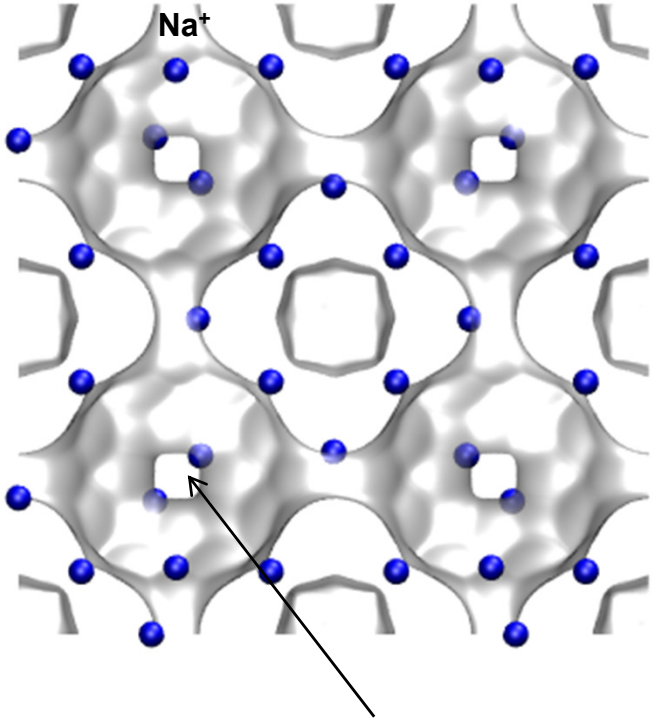

4.1 Å windows partially blocked by Na+ cations

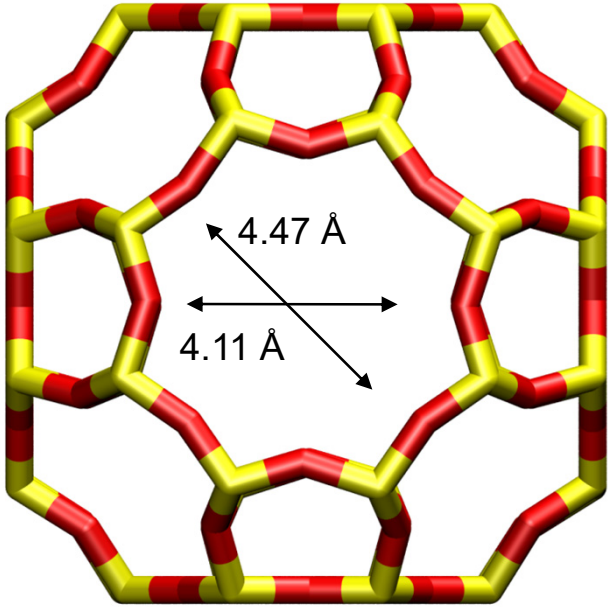

N_2 jumps lengthwise across windows and has the higher diffusivity

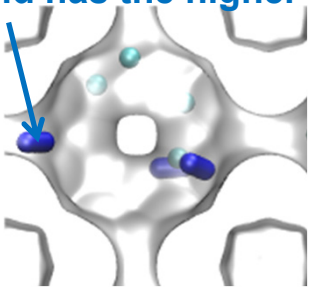

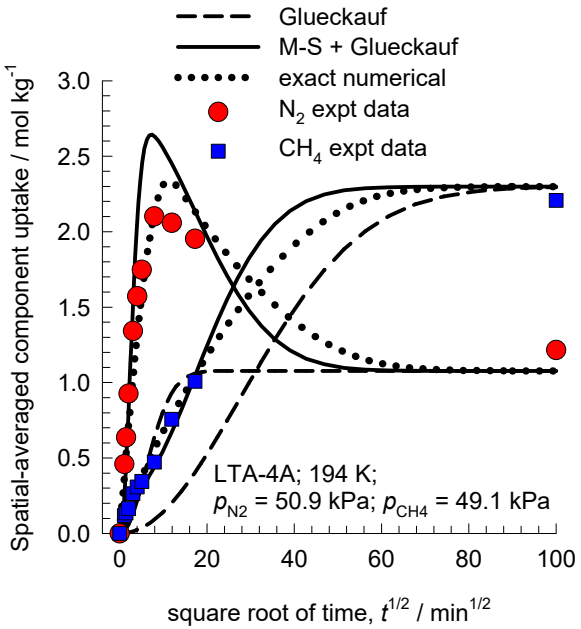

Figure S7

N_2/CH_4 mixture breakthrough in fixed bed with LTA-4A

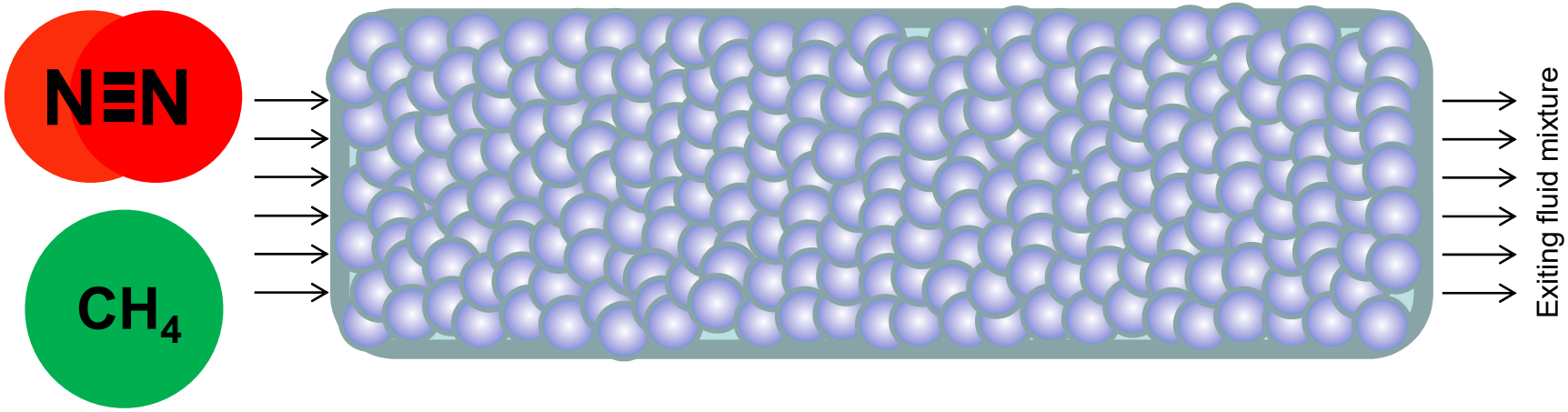

(a)

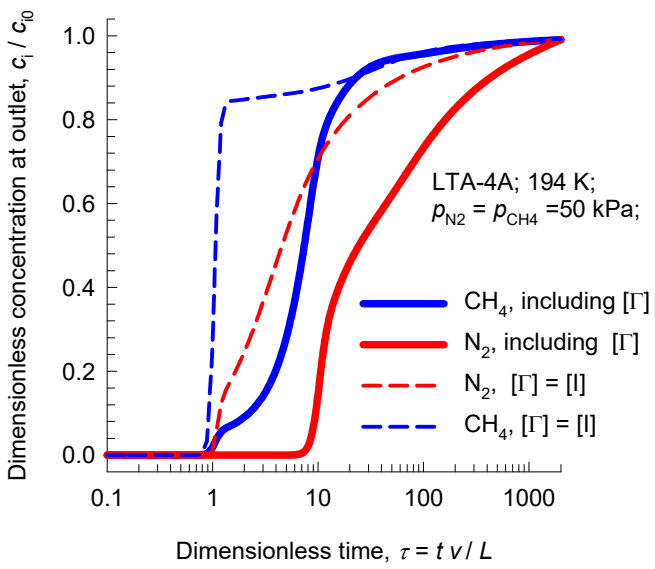

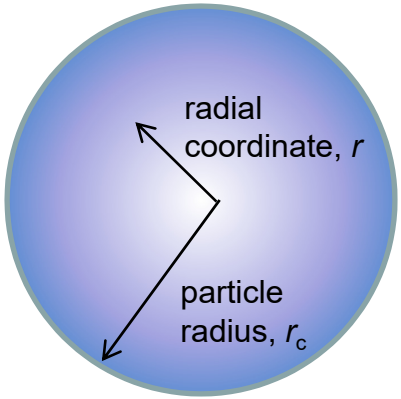

(b)

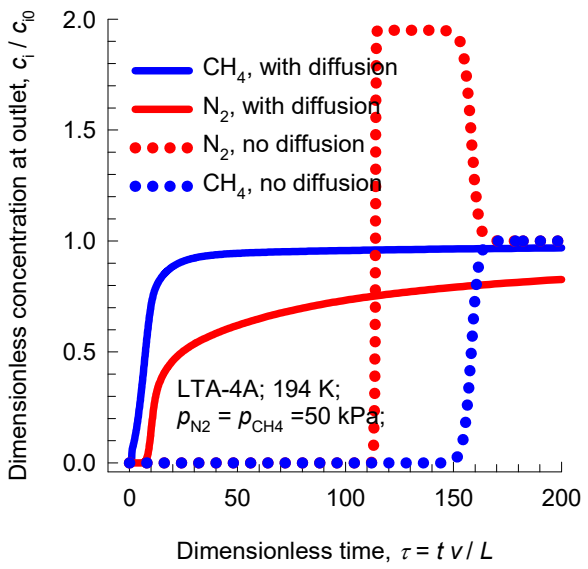

Figure S8

Transient ethanol/1-propanol uptake in SAPO-34

(a) Experimental data

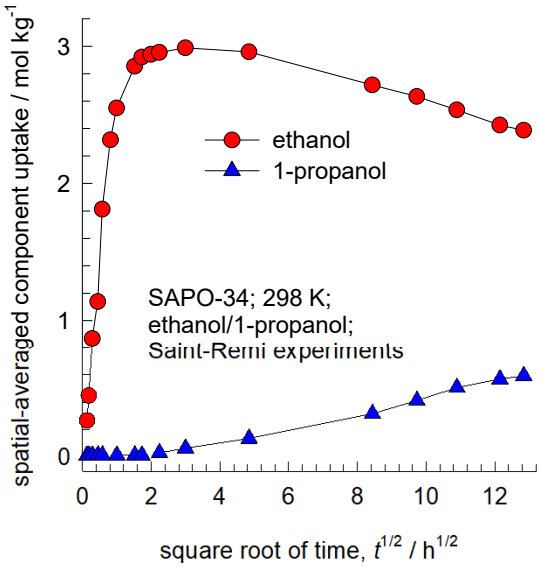

CHA structure

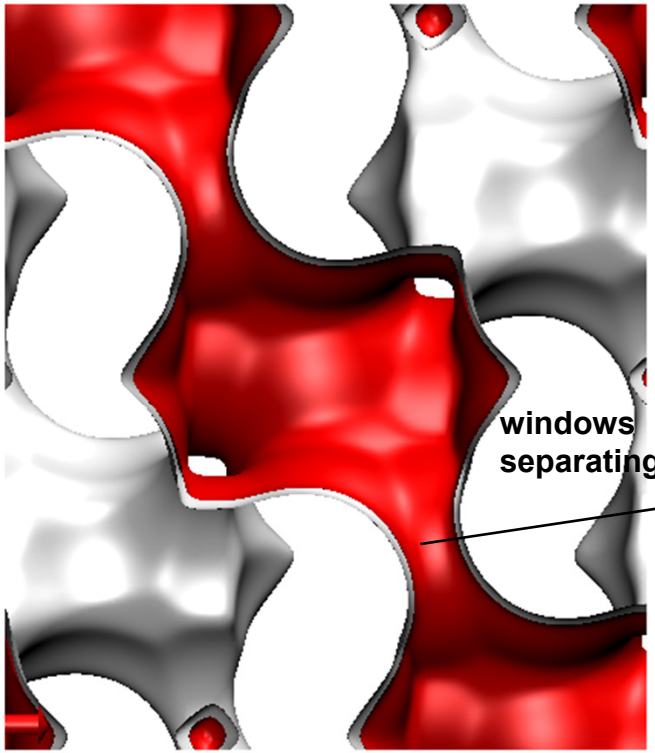

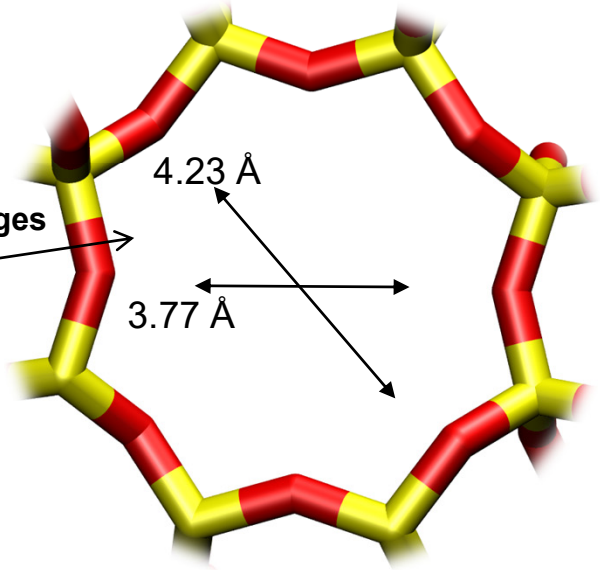

(b) Experimental data vs Transient Simulations

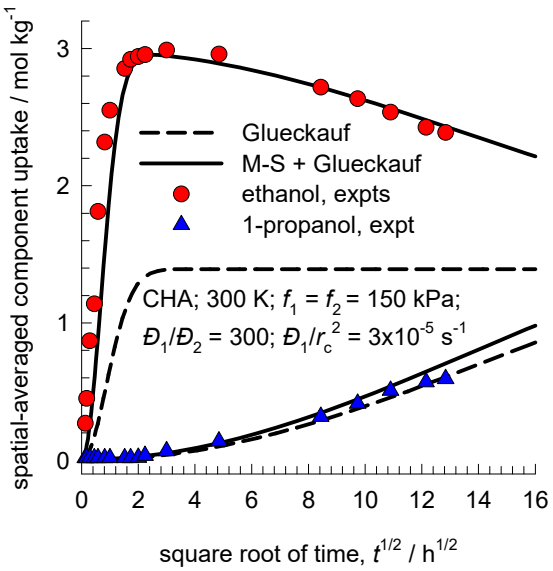

CBMC simulations of adsorption

Figure S9

(a) Unary isotherms

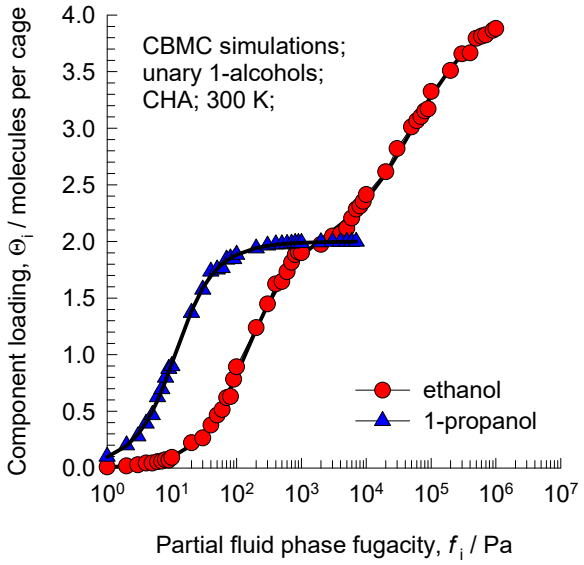

(c) CBMC vs IAST

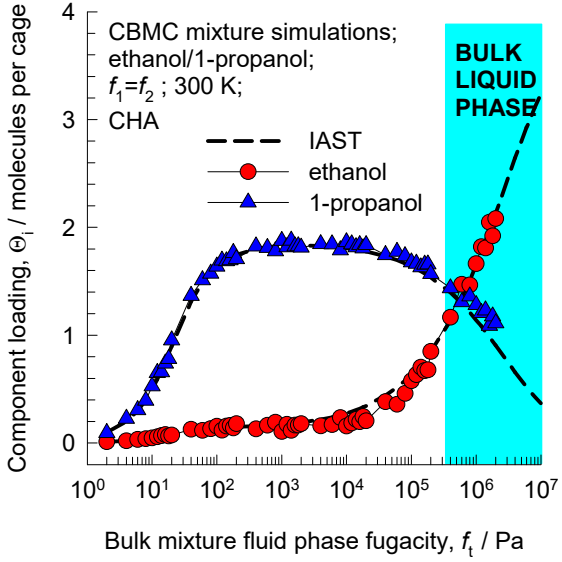

(b) Computational snapshots

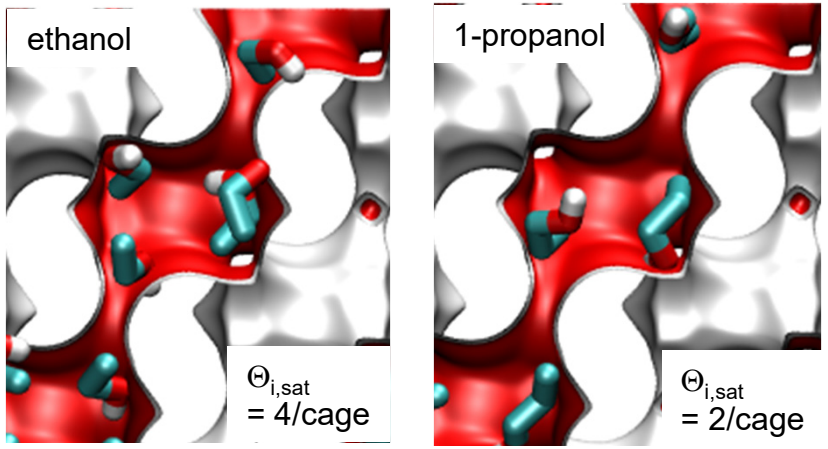

Figure S10

Experimental transient breakthroughs in fixed bed of SAPO-34

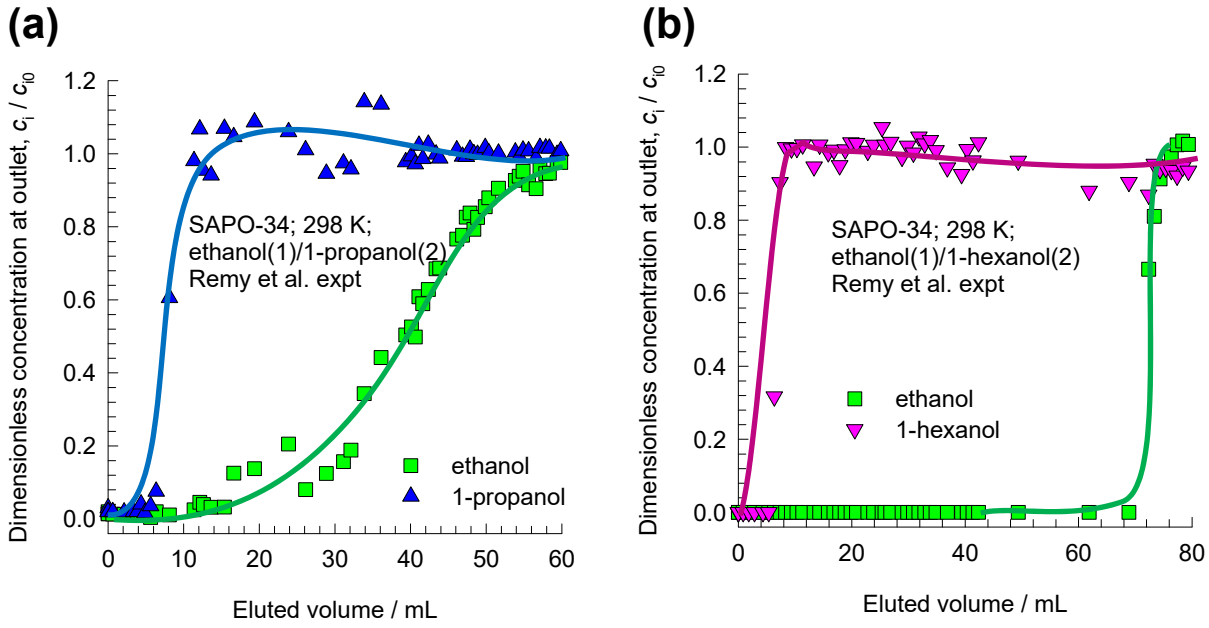

Transient uptake of nC4/iC4 within MFI crystal

Figure S11

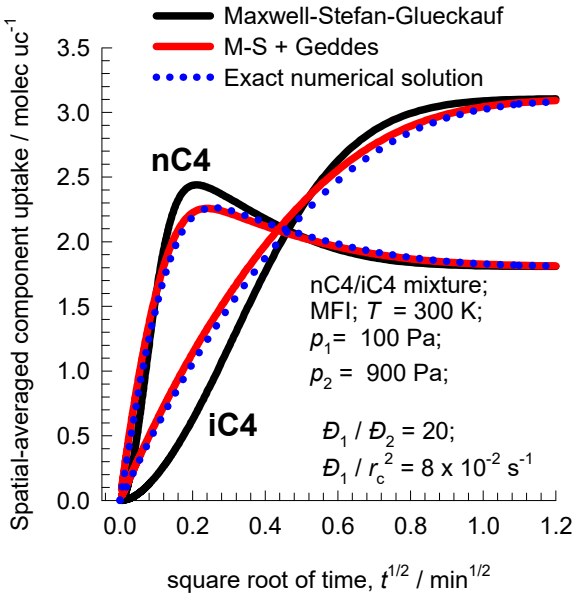

x-z view

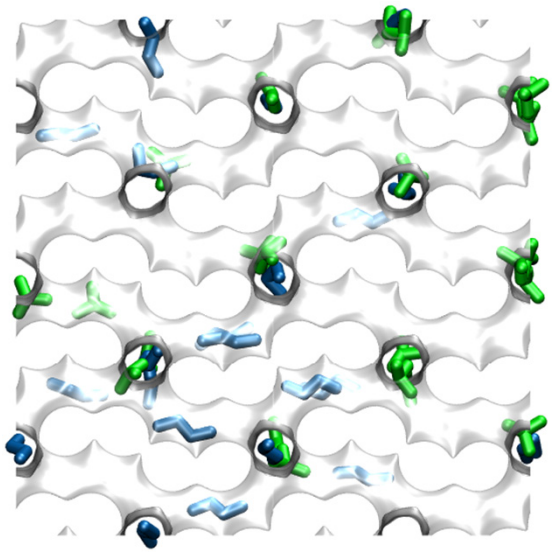

x-y view

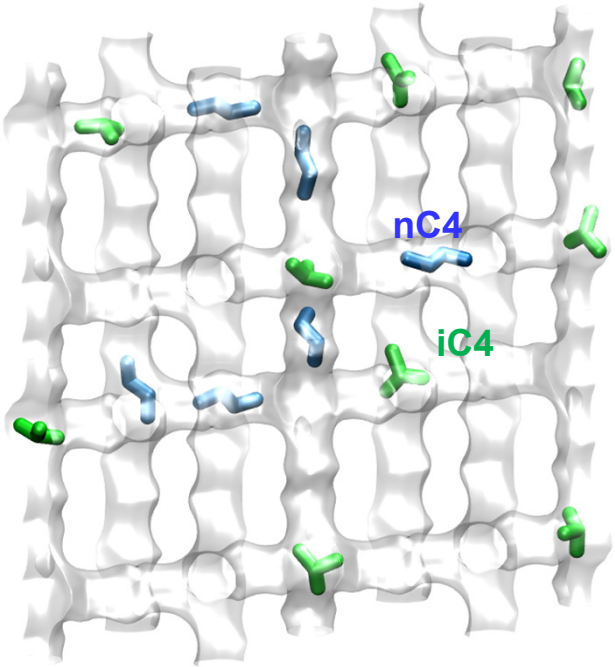

Figure S12

Transient O_2/N_2 uptake in LTA-4A

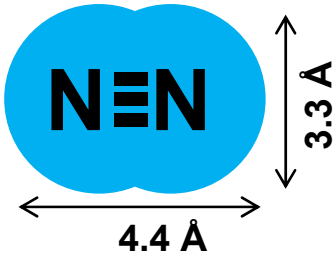

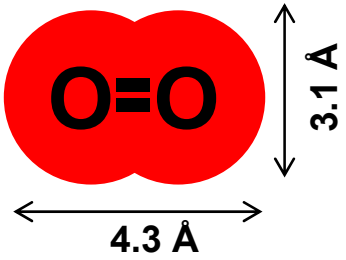

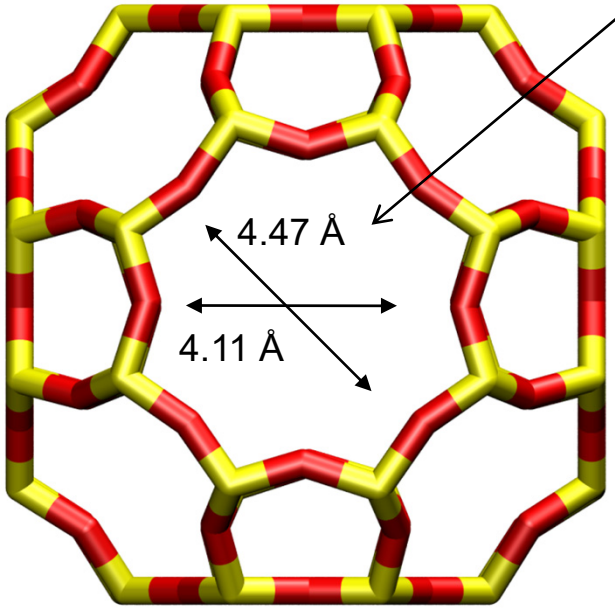

LTA-4A (96 Na+)

4.1 Å windows partially blocked by Na+ cations

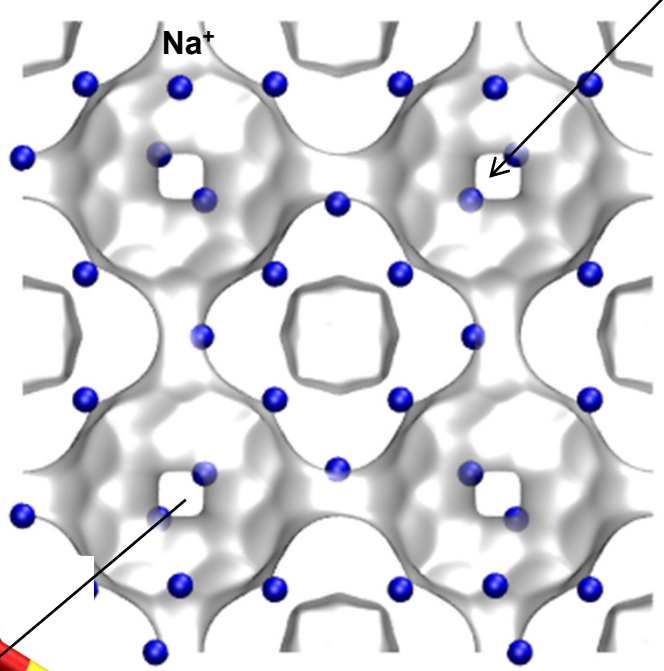

O_2 has the small cross-section and higher diffusivity

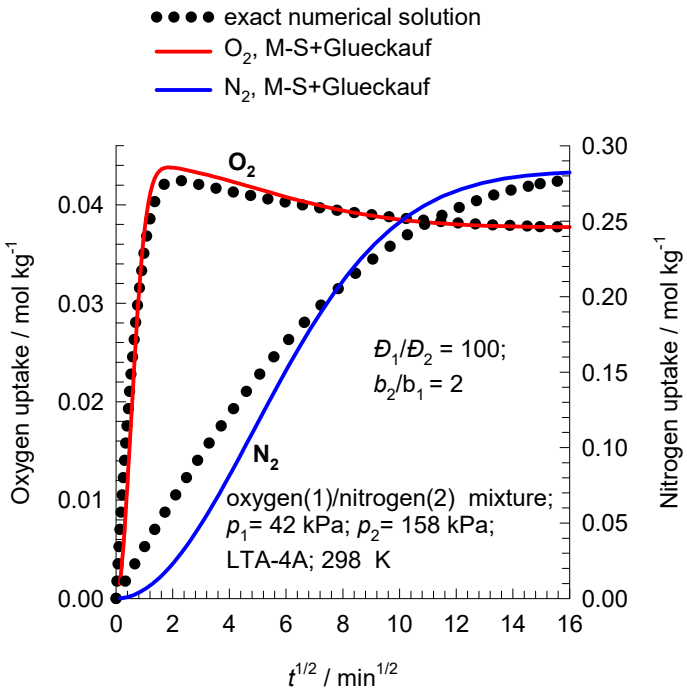

Figure S13

LTA-4A for N_2 production

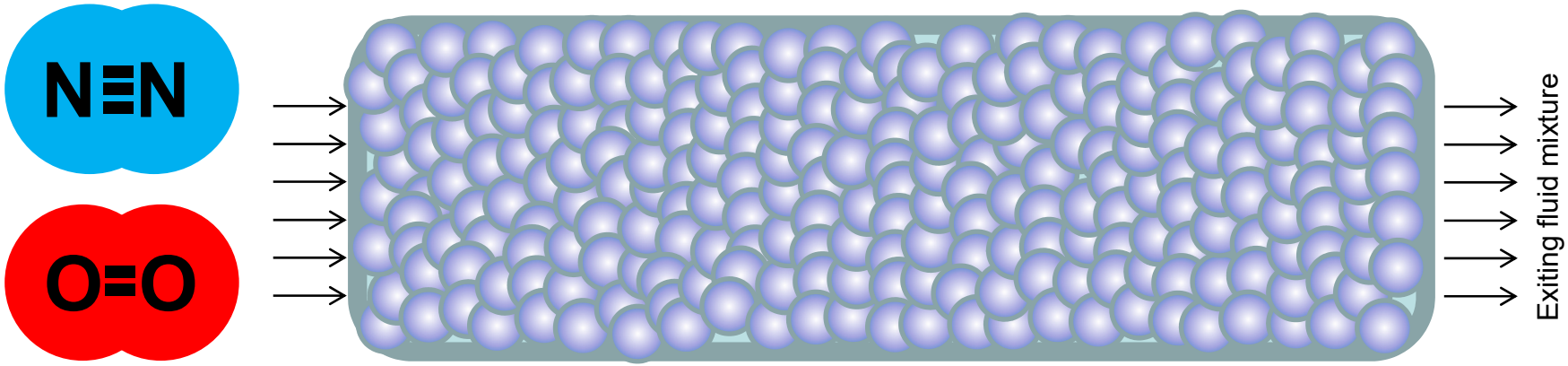

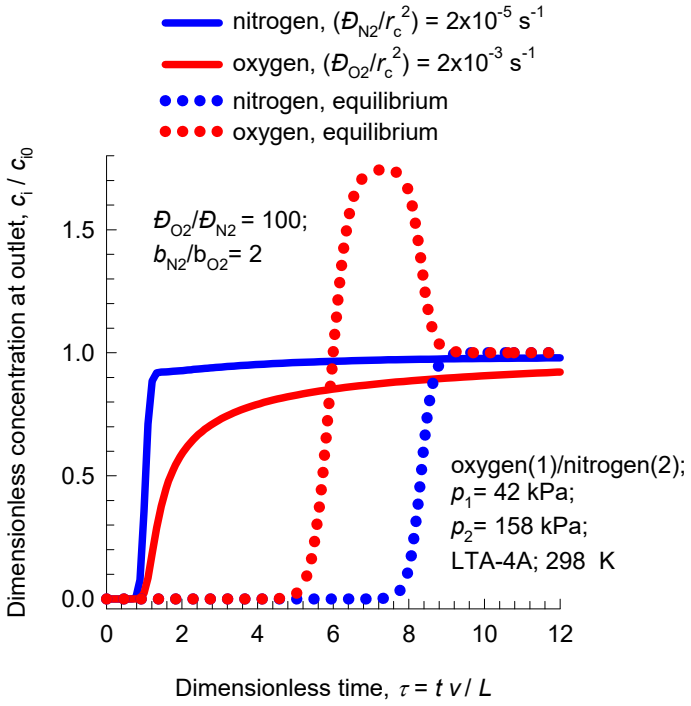

Figure S14

Propene/propane uptake in ZIF-8

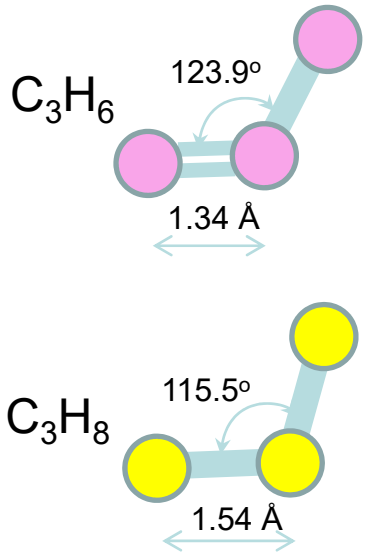

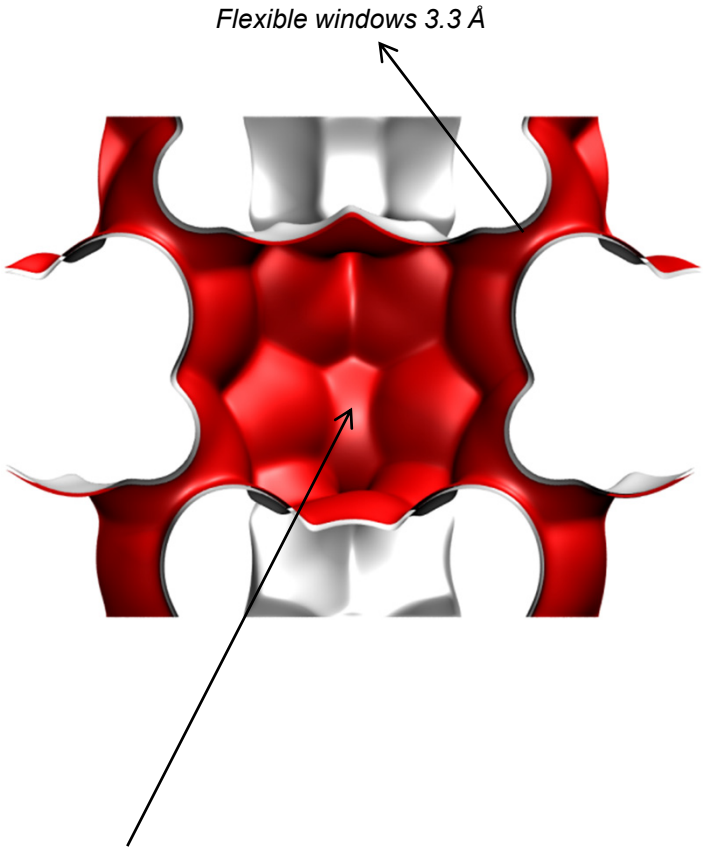

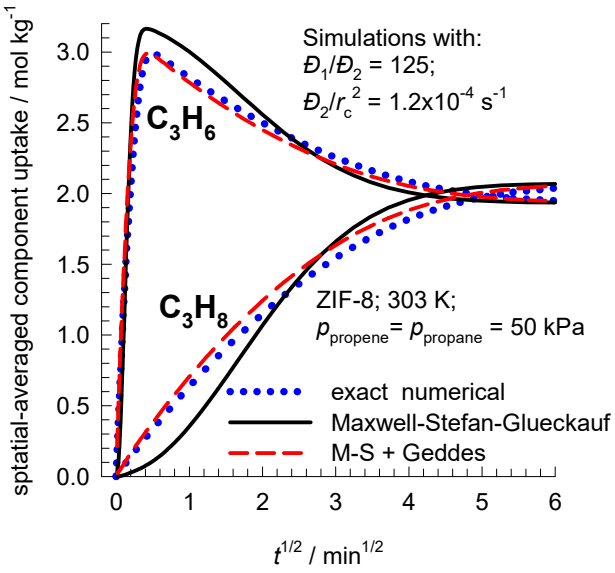

There are 2 cages per unit cell. The volume of one ZIF-8 cage is 1168 Å^3, significantly larger than that of a single cage of DDR (278 Å^3), or FAU (786 Å^3).

C_3H_6/C_3H_8 permeation across ZIF-8 membrane

Figure S15

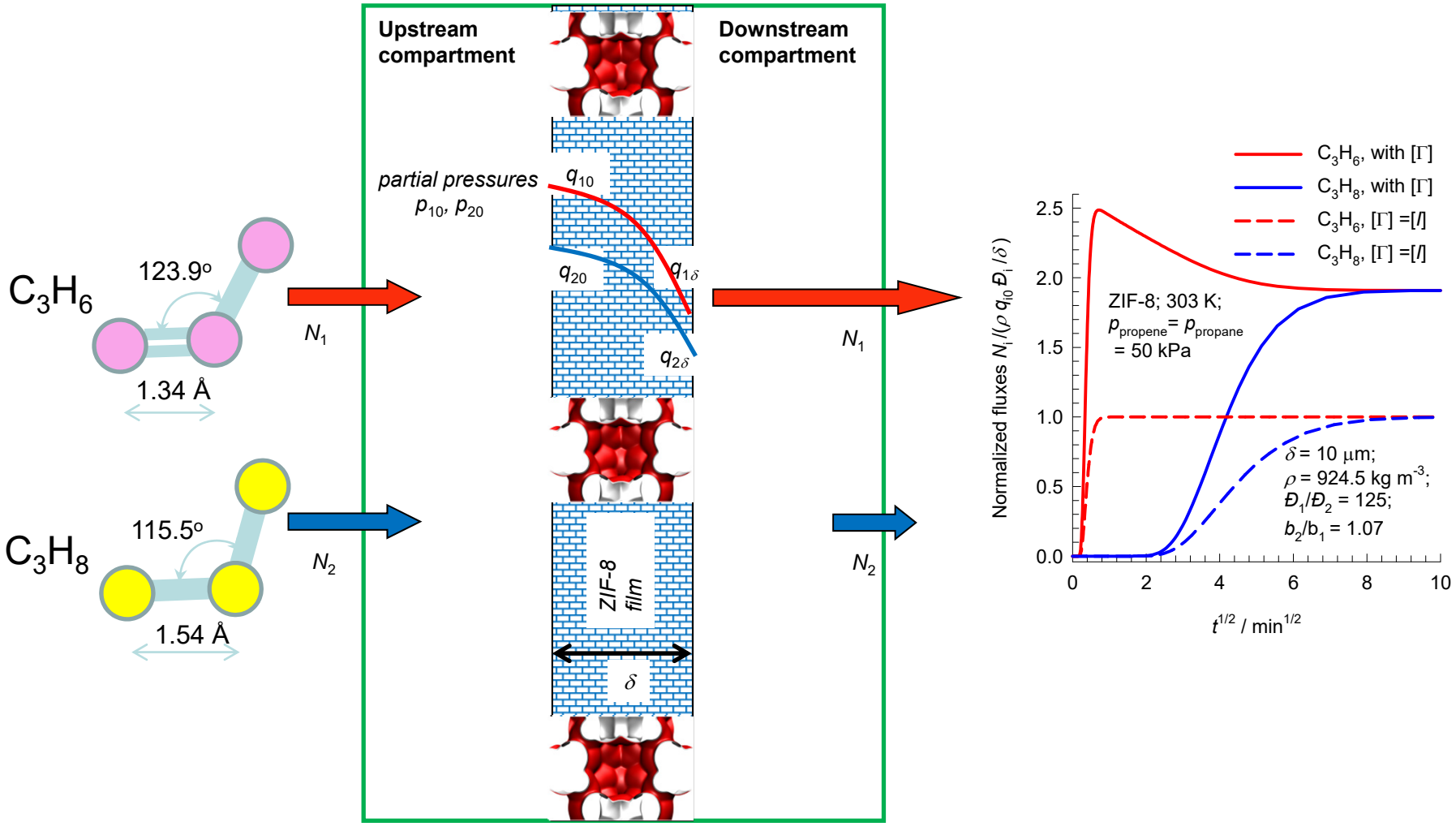

Figure S16

Transient Kr/Xe uptake in SAPO-34

CHA structure

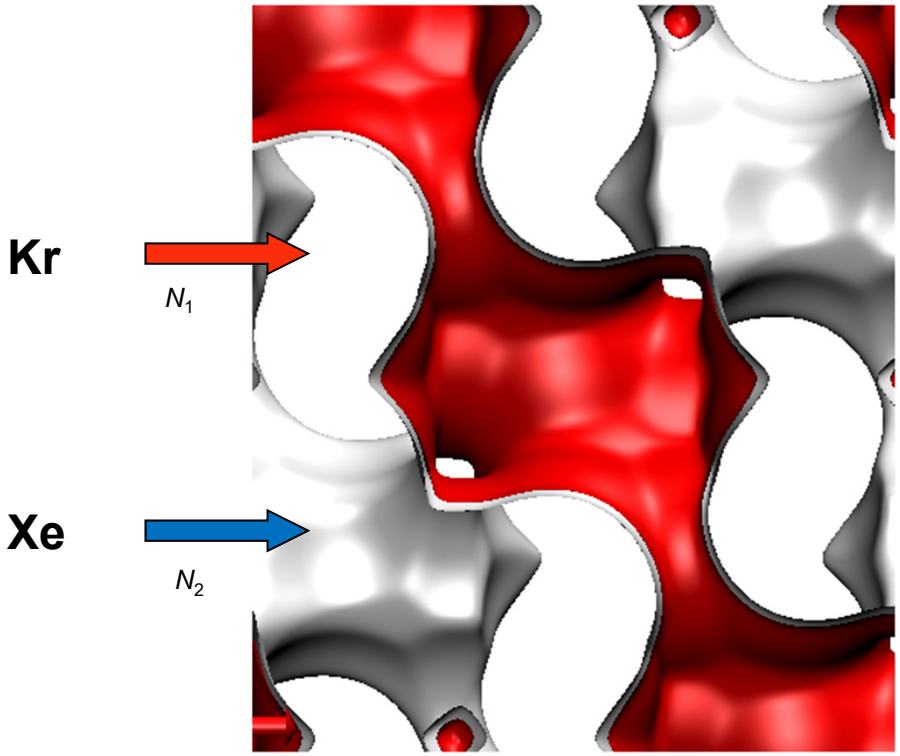

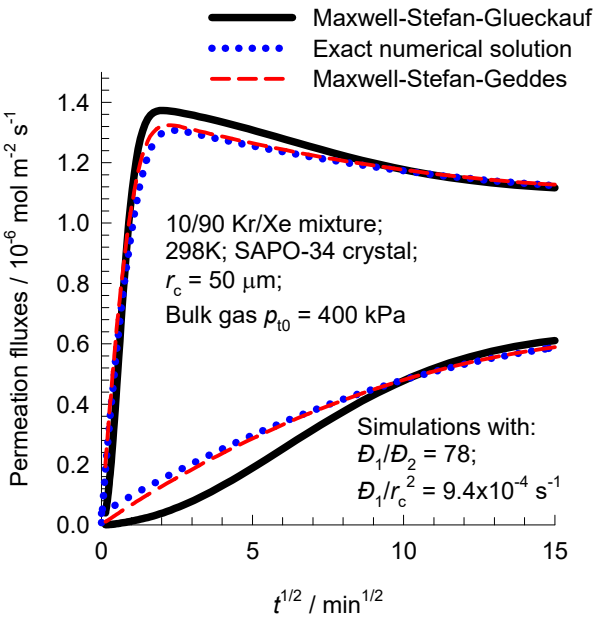

Figure S17

Transient Overshoot: Kwon isotherm data